

Ordering dynamics of one-dimensional Bloch wall system and domain size distribution function

Hiroki Tutu*

Applied Analysis and Complex Dynamical Systems, Graduate School of Informatics, Kyoto University, Kyoto 606-8501, Japan

(Received 10 July 2002; revised manuscript received 6 December 2002; published 21 March 2003)

The dynamics of domain size distribution in the ordering process for a one-dimensional classical anisotropic XY model is studied with a reduced equation of motion for the assembly of domain sizes. The system possesses two types of the domain wall structures, the Néel or Bloch walls, depending on the strength of magnetization anisotropy. In the Néel wall situation the neighboring walls interact with one another in only an attractive way. On the other hand, in the Bloch one, these walls interact in either an attractive or a repulsive way depending on their chiralities. For the Bloch wall situation, we found that the domain size distribution is characterized by solitonlike translational motion with a function form $h(y - y(t))$ and a characteristic domain size $y(t)$ for the domain size y . This is in contrast to that in the Néel wall situation, which can be described as a scaling-type distribution function $g[y/l(t)]/l(t)$, as was obtained by Nagai and Kawasaki, with a certain scaling length $l(t)$. We discuss why such a solitonlike motion appears instead of the scaling-type distribution function, show a proof for the absence of the scaling-type distribution, a qualitative estimation for the distribution function in the Bloch wall situation, and an analysis for the realization probability of a specified twistness.

DOI: 10.1103/PhysRevE.67.036112

PACS number(s): 64.60.Cn, 75.60.Ch, 05.20.Dd

I. INTRODUCTION

Phase ordering processes of various systems quenched from the homogeneous phase into a broken-symmetry phase have been widely studied for the last several decades [1–3]. The dynamical behaviors in such ordering process are described by the motion and the coarsening of defects, walls, or other kinds of topological singularities depending on the symmetries of their order parameters. An important aspect of such ordering process is that the statistical quantities of those systems are scaled with a single-length scaling parameter $l(t)$, which corresponds to the mean distance between such topological singularities or the mean diameter of domain sizes, and diverges in the course of time. In the majority of such systems it is well accepted that the statistical quantities involving a length scale variable, e.g., y , exhibit scale invariance by use of the single-length scaling $y/l(t)$. Some examples exhibiting such scaling behavior are droplet growth in binary mixture systems [4,5] and breath figures [6]. However, not all the systems undergoing such ordering process behave in self-similar ways, and there is a special case not obeying scaling behavior.

In this paper, we consider the statistical dynamics of domain sizes in the phase ordering process quenched from the disordered phase into the broken-symmetry phase in the dynamics governed by the time-dependent Ginzburg-Landau (TDGL) equation without thermal noise for a classical one-dimensional (1D) anisotropic XY-spin system. The Ginzburg-Landau free energy for the 1D anisotropic XY-spin system in the broken-symmetry phase is given by

$$\mathcal{H}\{\psi, \psi^*\} = \int dx \left[-|\psi|^2 + \frac{1}{2}|\psi|^4 - \frac{\gamma}{2}(\psi^2 + \psi^{*2}) + \left| \frac{\partial \psi}{\partial x} \right|^2 \right], \quad (1.1)$$

where x is the one-dimensional coordinate, ψ is the complex order parameter, and γ is the strength of magnetization anisotropy (without loss of generality γ is chosen to be positive, so that the easy axis equals the real axis). The equation of motion is given by the TDGL equation,

$$\dot{\psi}(x,t) = - \frac{\delta \mathcal{H}\{\psi, \psi^*\}}{\delta \psi^*(x,t)} = \psi - |\psi|^2 \psi + \gamma \psi^* + \frac{\partial^2 \psi}{\partial x^2}, \quad (1.2)$$

by which the free energy decreases monotonically, i.e., $d\mathcal{H}\{\psi, \psi^*\}/dt \leq 0$.

It is well known that a domain wall has different structures depending on the strength of anisotropy [7]: in a weak anisotropy region ($0 < \gamma < 1/3$) the stable domain wall is the so-called Bloch wall, on the other hand, in a strong anisotropy region ($\gamma > 1/3$), the so-called Néel wall is stable. Hereafter, we refer to these regimes as Bloch and Néel wall regimes, respectively. The characteristics of the Bloch wall is its chirality, which is the degrees of freedom corresponding to the clockwise or counterclockwise rotation of the phase of the complex order parameter. In the dynamics governed by Eq. (1.2), the interaction of neighboring Bloch walls with the same chirality is repulsive, while that with opposite ones is attractive, and the pair annihilates when their distance becomes sufficiently close. The repulsive interaction feature in the Bloch wall regime is in contrast to the Néel wall regime, in which walls always behave in attractive ways. Reflecting the difference in the interaction properties between walls, it is expected that there are different types of statistical behavior for assemblies of domain sizes between both regimes.

In a previous work [8], done by the author and Fujisaka, the evolution equation for the domain sizes in the Bloch wall situation was derived from the TDGL equation and the fundamental properties of the domain wall dynamics were investigated; there the dynamics of domain size distribution function (DSDF) were calculated numerically, and the DSDF

*Electronic address: tutu@i.kyoto-u.ac.jp

for the different types of domain, classified by the combination of neighboring chiralities, were found to show different behavior. The qualitative property of the structural factor was also investigated. However, our numerical result was limited to the early stage of the domain size kinetics. The present study deals with the long term behavior of the DSDF in the Bloch wall situation by using both numerical and analytical calculations.

The DSDF for the Néel wall situation is practically identical with that for nonconserved bistable systems. Nagai and Kawasaki (NK), and NK and Ogawa [9–12], studied the dynamics of the DSDF and the structure factor in the ordering process governed by the TDGL equation corresponding to the 1D Ising-spin system a couple of decade ago. Their approach was based on the following equation of motion for the sizes of domains. Letting the size of the i th domain be y_i , its growth is described by the equation

$$\dot{y}_i = e^{-y_{i-1}} + e^{-y_{i+1}} - 2e^{-y_i}, \quad (1.3)$$

together with the annihilation process: when a domain size becomes less than a cutoff size, the three adjacent domains merge and yield a new domain. NK obtained the exact form of the DSDF as a scaling form $g[y/l(t)]/l(t)$ from the kinetic equation made from Eq. (1.3). Rutenberg *et al.* [13] also derived the DSDF by another simplified treatment (see also Ref. [14]). Due to the exponentially decaying force, the average domain size exhibits a logarithmic growth behavior, $l(t) \sim \ln t$, which was also observed by experiments [15–18] for nearly 1D magnetic material.

For the 1D isotropic XY -spin model, Rutenberg *et al.* [19] discussed dynamical scaling for some types of order parameter correlation functions. For the 1D anisotropic XY -spin model, however, studies close to the present subject seem absent.

In this paper, we will show that the DSDF in the Bloch wall regime obeys a *solitonlike* translational motion, and that the DSDF can be written in the function form $h(y - y_d(t); t)$ [it can be written as $h(y - y_d(t))$ in a good approximation], where the peak position $y_d(t)$ grows as $y_d(t) \sim \ln t$ and the width of the peak seems to saturate to a constant value. The main aim of the paper is to elucidate the origin of the solitonlike motion and to obtain the qualitative form of the function h .

The paper is organized as follows. In Sec. II, we briefly introduce the evolution equation for domain sizes and show its qualitative properties. In Sec. III, we present our numerical analysis of the DSDF. In Sec. IV, the master equation for the DSDF is derived, and the realization probability for twistness configuration is also obtained. In Sec. V, we analyze the single domain size distribution function. There are two subsections. First, we will prove that the scaling-type solution is absent for the Bloch wall regime. In the same approach, as the studies by NK, we consider the kinetic equation for domain size assuming the scaling form for its solution; however, it will be found that the equation leads to the divergence of the first moment, that being inconsistent with the scaling assumption. Second, with an alternative approach incorporating the correlation effect between domains,

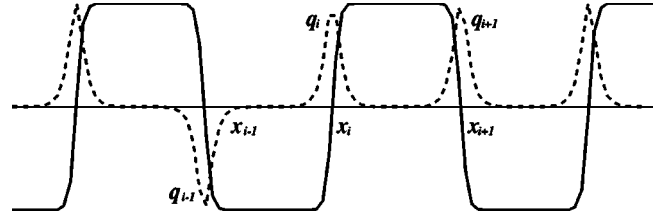


FIG. 1. Definition of variables.

we will obtain an Fokker-Planck-type equation and its solution corresponding to the solitonlike behavior. In Sec. VI, we will discuss the differences of the DSDFs between Néel and Bloch wall situations. Finally, we summarize our results in Sec. VII.

II. DYNAMICS OF BLOCH WALLS

The profile of the Bloch wall, with the center being at $x = x_0$, is obtained as a stationary solution of Eq. (1.2) with the boundary condition $\psi(x \rightarrow \pm\infty) = \pm\sqrt{1+\gamma} \equiv \pm X_0$ ($\gamma > 0$), $\pm X_0$ being the uniform solutions of Eq. (1.2), i.e.,

$$\psi_B(x) = pX_0 \tanh[(x - x_0)/\xi] + iqY_0 \operatorname{sech}[(x - x_0)/\xi], \quad (2.1)$$

where $Y_0 = \sqrt{1-3\gamma}$, $\xi = 1/\sqrt{2\gamma}$ (the characteristic width of wall), p and q , respectively, take signs of either $+1$ or -1 . With the quantity pq , which is referred to as the chirality of the wall, one can distinguish the rotation direction of coarse-grained spins on a wall.

The ordering process of the present system is described as the motion of walls and the pair annihilation of neighboring walls with an opposite chirality. As sketched in Fig. 1, let us denote the i th wall position as x_i and its chirality as $(-1)^i q_i$, where the factors $(-1)^i$ and q_i are, respectively, equivalent with the role of p and q in Eq. (2.1). In addition, let us introduce the i th domain size $y_i = x_{i+1} - x_i$ and its *twistness* $Q_i = q_{i+1}q_i$, which indicates whether the i th domain is twisted ($Q_i = -1$) or untwisted ($Q_i = 1$). The number of domains runs from 1 to $N(t)$ with $N(t)$ being the total number of domains at time t , and, in this paper, we impose the periodic boundary condition in which the $[i+N(t)]$ th domain is identical to the i th domain.

The growth velocity of the i th domain size has been approximately obtained as

$$A \frac{dy_i}{dt} = Q_{i+1} e^{-y_{i+1}/\xi} + Q_{i-1} e^{-y_{i-1}/\xi} - 2Q_i e^{-y_i/\xi}, \quad (2.2)$$

where $A = (1 - \gamma/3)/[4\sqrt{2\gamma}(1 - 3\gamma)]$ [8]. Equation (2.2) has also been derived from the dissipative 1D sine-Gordon model by Kawasaki and Ohta [20]. In the derivation of Eq. (2.2), we neglected the higher order powers of any exponential force smaller than $e^{-y_i/\xi}$. The pair annihilation of neighboring walls must be taken into account if a domain size reaches the cutoff size y_c ($\sim \xi$), i.e., when the k th domain

size becomes $y_k = y_c$, three consecutive domains, $(k-1)$ th, k th, and $(k+1)$ th with $Q_k = 1$, are merged into one domain and they are rearranged as

$$y_{k-1} + y_c + y_{k+1} \rightarrow y_{k'}, \quad (2.3)$$

$$Q_{k-1} Q_k Q_{k+1} (= Q_{k-1} Q_{k+1}) \rightarrow Q_{k'}.$$

For the case of the isolated domain, consisting of only a pair of walls, with size y and twistness Q , Eq. (2.2) gives

$$A \dot{y} = -2Q e^{-y/\xi}, \quad (2.4)$$

and its solution is obtained as $y(t) = \xi \ln(e^{y(0)/\xi} - 2Qt/A)$ with the initial size $y(0)$. Thus, the size of the twisted domain ($Q = -1$) grows, while that of the untwisted domain ($Q = 1$) shrinks and eventually disappears. From a physical point of view, this concerns the twist energy of spins.

It is also noted that the time scale of Eq. (2.2) goes to infinity on the transition point $\gamma = 1/3$ between Néel and Bloch walls. In such a case, higher order terms than $e^{-y_i/\xi}$ become relevant. However, in this paper we do not deal with such a critical situation. For later convenience, we write down here the dimensionless form of Eq. (2.2), y_i and t being scaled as $y_i/\xi \rightarrow y_i$ and $t/(\xi A) \rightarrow t$,

$$\frac{dy_i}{dt} = Q_{i+1} e^{-y_{i+1}} + Q_{i-1} e^{-y_{i-1}} - 2Q_i e^{-y_i}. \quad (2.5)$$

The fundamental properties of the domain size dynamics are as follows. In the dynamical process we have two conservation quantities, the total domain size $\sum_i^{N(t)} y_i = L$ (L , the system size) and the total winding number

$$W = \sum_i^{N(t)} (-1)^i q_i, \quad (2.6)$$

which multiplied by π is the net phase difference between boundaries. The later is the consequence of the topological invariance for the elimination of the untwisted domains, because the elimination of the k th untwisted domain ($Q_k = q_k q_{k+1} = 1$) sandwiched between k th and $(k+1)$ th walls for which $-q_k + q_{k+1} = 0$ holds does not change W . In a statistical argument in Sec. IV B, it is also shown that the ensemble average of the quantity $\sum_i^{N(t)} Q_i / N(t)$ is a monotonically decreasing quantity. By using the central limit theorem, W is estimated as $W^2 \sim N(0)$ for large $N(0)$.

In order to see the role of $\{Q\}$ when many domains are present, let us consider the linear stability of the state in which all domains have the same size \bar{y} and the same twistness Q . Letting δy_i be the deviation from \bar{y} for the i th domain size, the linearized equation for δy_i is given by

$$\xi A \delta \dot{y}_i = -Q e^{-\bar{y}/\xi} [\delta y_{i+1} + \delta y_{i-1} - 2\delta y_i]. \quad (2.7)$$

Equation (2.7) indicates the negative (positive) stiffness for the case $Q = 1$ ($Q = -1$). The uniform state is therefore unstable (stable) for $Q = 1$ ($Q = -1$). This suggests that domain sizes develop their size fluctuation by an attractive

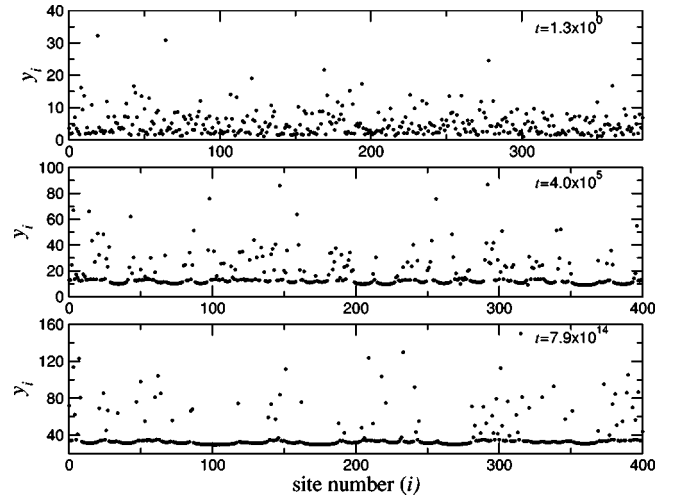


FIG. 2. The evolution of domain sizes $\{y_i(t)\}$ ($i = 1, \dots, 400$). The vertical and horizontal axes indicate the length of the domain size and the array index of domains, respectively. Each snapshot shows the configuration of consecutive domain sizes at each of the different times $t = 1.3$, $t = 4.0 \times 10^5$, and $t = 7.9 \times 10^{14}$, in order from top to bottom.

force in the case $Q = 1$, or they retain equal intervals among walls by a repulsive one of the case $Q = -1$. Figure 2 shows the temporal evolution of consecutive domain sizes, which are generated by Eq. (2.5) for the randomly distributed initial sizes by keeping their average equal to 4.0 and initial twistness with an equal probability for each state. Details of the method of calculation are explained in Sec. III. Each snapshot shows the configuration of consecutive domain sizes $y_i(t)$ ($i = 1, \dots, 400$) at each of the three successive times in order from top to bottom. These snapshots show the development of clusters, where each of the clusters consists of equal size domains and increases its population by absorbing more domains, being of $Q = -1$, arising from the annihilation of untwisted domains, at both sides. This behavior is well explained by the linear stability argument mentioned above.

III. NUMERICAL ANALYSIS

The direct integration of Eq. (2.5) by the usual Runge-Kutta methods spends too much time to complete the entire kinetic stage, because the calculation speed becomes slow in a logarithmic time scale. For the purpose of efficient integration, the present study uses the *variable time step* algorithm. Equation (2.5) is discretized as

$$y'_i(\tau + \Delta\tau) = y'_i(\tau) + [Q_{i+1} e^{-y'_{i+1}} + Q_{i-1} e^{-y'_{i-1}} - 2Q_i e^{-y'_i}] \Delta\tau, \quad (3.1)$$

where y'_i is $y'_i \equiv y_i - y_{\min}(t)$, i.e., the relative size measured from the minimum domain size $y_{\min}(t)$, and $\Delta\tau$ is the thickness of time defined by $\Delta t \equiv \Delta\tau e^{y_{\min}(t)}$. The unit of time is varied in accordance with the fastest process, and the time

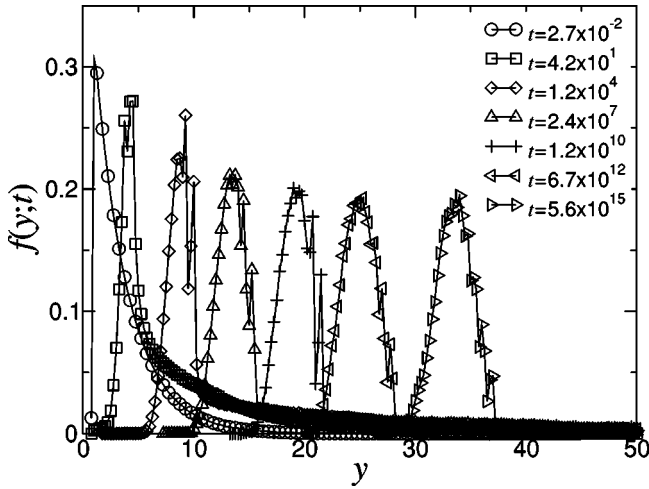


FIG. 3. Temporal evolution of $f(y;t)$. The vertical and horizontal axes indicate the values of $f(y;t)$ and domain size y , respectively. Different kinds of symbols correspond to snapshots at different times, the correspondences being indicated within the figure. The time intervals between successive snapshots are separated by an approximately logarithmic time order, so the snapshots are equally separated.

steps spent by the process until the collapse of the fastest domain are proportional to its size, which is simultaneously the smallest domain size $y_{min}(t)$. The whole algorithm is summarized in the following statements: (i) find the domain being the smallest size [$y_k(t) = y_{min}(t)$] with the positive twistness ($Q_k = 1$), (ii) guess the time steps spent until the occurrence of the next annihilation event, and do a numerical integration for those steps, (iii) if the annihilation event occurs [$y_k(t) < y_c$], return to (i) and add the time spent in that process to the real time t , or else go to (ii). In the present study, the numerical integration between successive annihilation events was done by the Runge-Kutta-Gill method.

The initial distributions for our calculations were prepared as follows: The initial sizes of domains $\{y_1, y_2, \dots, y_{N_0}\}$ were given randomly by the constraint $\bar{y}(0) = 4$ (bar denotes

the mean of all elements), and the initial values of twistness $\{Q_1, Q_2, \dots, Q_{N_0}\}$ were given randomly with an equal probability for each state, where $\bar{Q} \sim 0$ should be satisfied. The other parameters were chosen as follows: the initial number of domains, $N(0) \equiv N_0 = 2^{14}$, the number of samples for statistical average, $N_s = 204$, the cutoff size for domain sizes, $y_c = 1$, the time increment for the numerical integration, $\Delta\tau = 0.01$.

Figure 3 shows the temporal evolution of the DSDF,

$$f(y;t) = \left\langle \frac{1}{N(t)} \sum_i^{N(t)} \delta(y - y_i(t)) \right\rangle, \quad (3.2)$$

where $\langle \dots \rangle \equiv (1/N_s) \sum_s^{N_s} \dots$ denotes the average of the samples of different initial distributions with the sample number N_s , and $\delta(\dots)$ is the Dirac delta function. The time evolution of $f(y;t)$ is represented by the successively plotted curves consisting of different kinds of symbols, the kinds corresponding to different times. The initial distribution function takes an exponential form $f(y;0) \propto \exp[-(y - y_c)/(\bar{y} - y_c)]$, which is the manifestation that shows that the assembly of the initial wall positions obeys Poissonian statistics. After the early collapse of short size domains, one can observe a translational motion of the DSDF, i.e., the position of the peak temporally moves rightward in a logarithmic time scale $\sim \ln t$, and the height has a tendency to saturate into a constant value.

More detailed information can be obtained with the joint distribution function for y and Q ,

$$f(y, Q; t) = \left\langle \frac{1}{N(t)} \sum_i^{N(t)} \delta(y - y_i(t)) \delta_{Q, Q_i(t)} \right\rangle, \quad (3.3)$$

where δ_{Q, Q_i} is the Kronecker's delta. Figure 4(a) exhibits that $f(y, 1; t)$ decreases its peak height and broadens its peak width. This behavior may bring the expectation that $f(y, 1; t)$ has the same property as in the Néel wall situation, i.e., the scaling property. However, this expectation is not completely

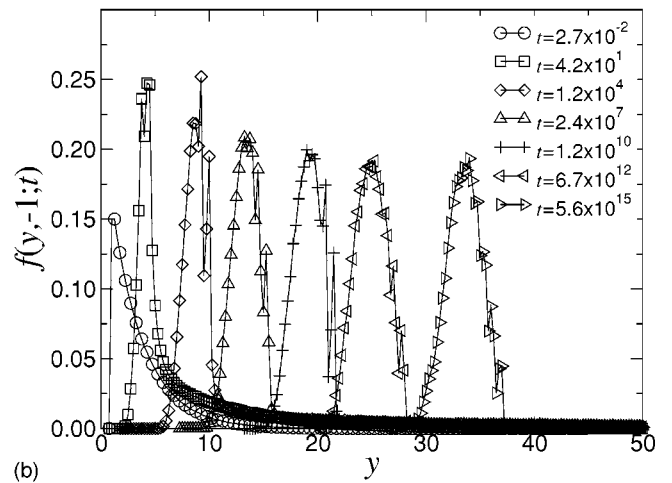
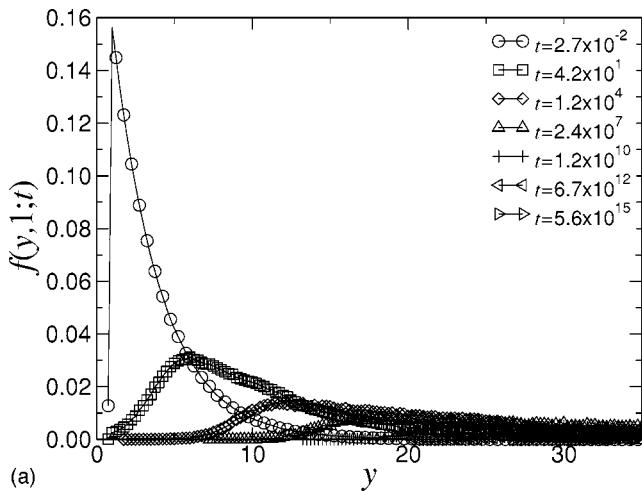


FIG. 4. Temporal evolution of $f(y, Q; t)$. Figures (a) and (b), respectively, show $f(y, 1; t)$ and $f(y, -1; t)$. The times of snapshots and the corresponding kinds of symbols are the same as those in Fig. 3.

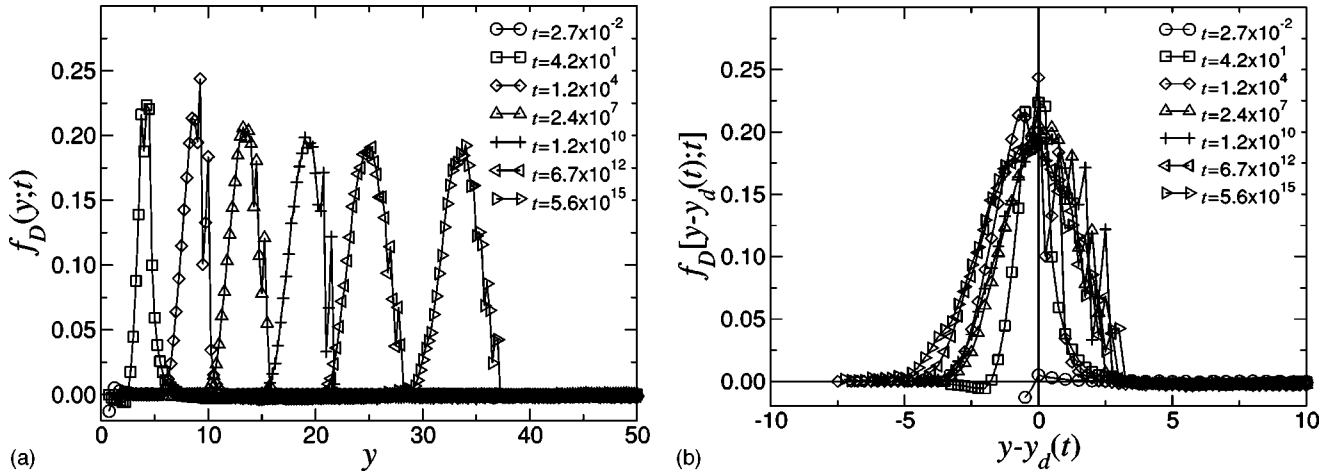


FIG. 5. (a) Temporal evolution of $f_D(y;t)$, and (b) its profiles for different times on the frame $y - y_d(t)$. The times of snapshots and the corresponding kinds of symbols are the same as those in Fig. 3.

realized, which will be shown in a later numerical (see the explanation below Fig. 6) and theoretical analysis (see Sec. V A). Figure 4(b) indicates that the drift motion observed in Fig. 3 is owing to the behavior of $f(y, -1;t)$. This implies that the DSDF $f(y, -1;t)$ can be written as $f(y, -1;t) \sim h(y - y_d(t))$ with $y_d(t)$ corresponding to the position of the peak and $h(z)$ being a function independent of time.

For the purpose of helping the present analysis, let us suppose that the DSDF (3.3) can be divided as

$$f(y, Q;t) = f^<(y, Q;t) + f^>(y, Q;t), \quad (3.4)$$

where the superscripts $<$ and $>$, respectively, signify the regions $y < y^*(t)$ and $y > y^*(t)$ with a size $y^*(t)$ separating behaviors of the DSDF. For the region $y > y^*(t)$, we assume that the domain size kinetics are governed by annihilation and creation process among domains, Eq. (2.3), and which break a Q -relevant memory effect among domains. Accord-

ingly, we can assume the distribution function $f^>(y, Q;t)$ for each Q not to depend on Q , i.e., $f^>(y, Q;t) \approx g(y;t)$. Then, we have

$$f(y, Q;t) = f^<(y, Q;t) + g(y;t). \quad (3.5)$$

We also assume that the dynamical evolution generated by Eq. (2.2) brings a Q -dependent effect for the domain size kinetics in the region $y < y^*(t)$, where twisted domains ($Q = -1$) tend to correlate in their neighboring sizes, while untwisted domains ($Q = 1$) disperse their sizes. This also leads to a sharpening ($Q = -1$) and broadening ($Q = 1$) of each DSDF in that region. Hence, the function

$$f_D(y;t) = f(y, -1;t) - f(y, 1;t) = f^<(y, -1;t) - f^<(y, 1;t) \quad (3.6)$$

extracts the Q -dependent part from both distributions.

Figure 5(a) shows the time evolution of $f_D(y;t)$. The

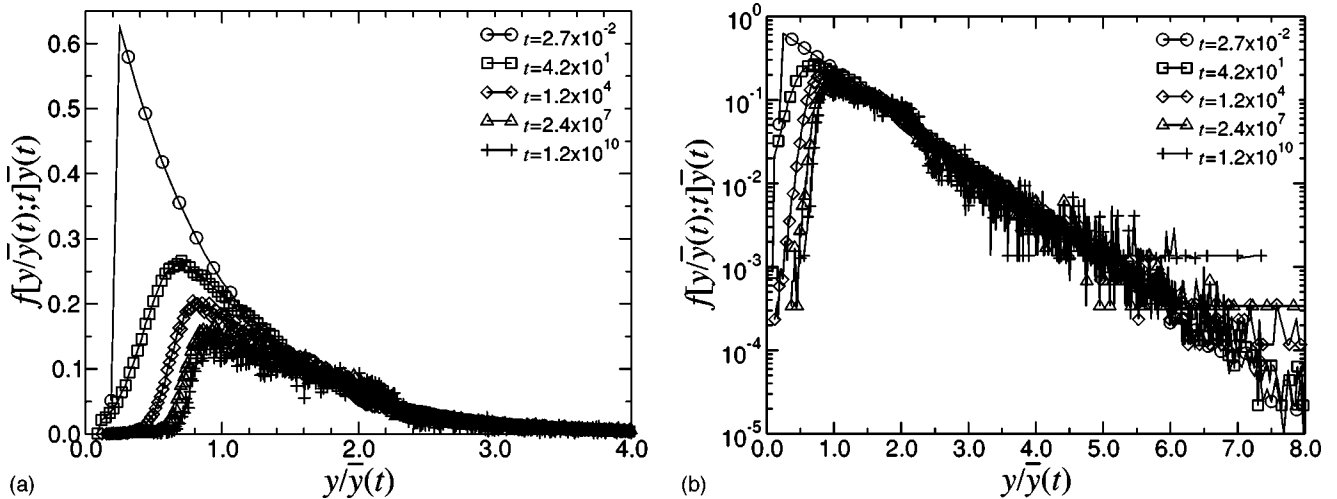


FIG. 6. (a) The result of the scaling (3.7) for $f(y, 1;t)$, and (b) its linear-log plot, where the vertical axis is the logarithmic scale. The last two pieces of data for $t = 6.7 \times 10^{12}, 5.6 \times 10^{15}$ used in the previous figures are dropped to maintain clarity, but the rest of the data are the same as those in Fig. 3.

function $f_D(y;t)$ obviously exhibits translational motion, in which the location of the peak moves with an equal speed in a logarithmic time scale, i.e., $y_d(t) \sim \ln t$. Figure 5(b) shows the evolution of $f_D(y-y_d(t))$ on the moving frame $y-y_d(t)$. The probability mass around $y \approx y_d(t)$ corresponds to the population of the domain sizes that compose the clusters as seen in Fig. 2. Reflecting the formation of the clusters, the total mass of $f_D(y-y_d(t))$ increases from zero and gradually saturates to a constant, where most of the mass of $f_D(y;t)$ comes from $f(y,-1;t)$, i.e., the DSDF for the small size region, $y < y^*(t)$, is dominated by $f^<(y,-1;t)$ [$f^<(y,-1;t) \gg f^<(y,1;t)$].

Another point of interest is what kind of statistical behavior describes $g(y;t)$. In order to see that, we have attempted the scaling form

$$f(y,1;t) \sim g(y/\bar{y}(t))/\bar{y}(t) \quad (3.7)$$

to $f(y,1;t)$ in Fig. 6, where we use $f(y,1;t)$ instead of $g(y;t)$, and Eq. (3.7) is the same type scaling as the Néel wall situation. For the scaling length, we have used the mean domain size $\bar{y}(t) = L/\langle N(t) \rangle$. Figure 6(a) shows the result of the scaling (3.7) for $f(y,1;t)$. Obviously in the small size region the scaling assumption (3.7) is broken. Figure 6(b) is the linear-log plot of Fig. 6(a). $f(y,1;t)$ has the exponentially decaying part written as $\sim e^{-1.2y/\bar{y}(t)}/\bar{y}(t)$ for the large size region $y/\bar{y}(t) > z_c(t)$, where $z_c(t) \approx 2.0$ for the last data in Fig. 6(b), and $z_c(t)$ gradually increases in the course of time. These results imply that $f(y,1;t)$ is no longer written in an entire scaling form, instead, it is considered that the exponential-type scaling form with the characteristic size $\bar{y}(t)$ for $f(y,1;t)$ transiently appears for the large size region and gradually collapses away from the side of the small size region. The intuitive explanation for that is as follows. Let us consider the arrangements of Q for three consecutive domains to be able to create a positive- Q domain after the collapse of the middle domain. Then, such arrangements are found to be (1,1,1) and (-1,1,-1), where (Q_1, Q_2, Q_3) denotes the arrangement of twistness for three consecutive domains. Similarly, let (y_1, y_c, y_2) be the configuration of the domain sizes just before collapse. When either of y_1 or y_2 is sufficiently large, the resultant domain may bring no memory or correlation effect relevant to Q since the dynamics of larger domains is governed by the annihilation process (2.3), which breaks the dynamical memory or correlation effect. On the other hand, when both y_1 and y_2 are small, the annihilation event $(-1,1,-1) \rightarrow 1$ can accumulate the correlation effect among domain sizes to $f(y,1;t)$, and the event $(1,1,1) \rightarrow 1$ elevates the correlation effect toward the larger size region. This is because the dynamics corresponding to the DSDF $f^<(y,-1;t)$ condenses the clusters in which all domains have same twistness and are equally sized around the characteristic size $y_d(t)$, and the form of $f^<(y,-1;t)$ is not a scaling form but the solitonlike form, $h(y-y_d(t))$, whose width is almost constant. As a consequence, the exponential-type scaling form for $g(y;t)$, which is settled through a large number of annihilation events in early stages

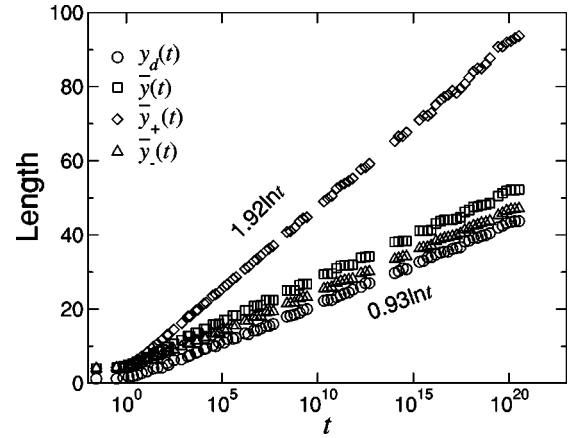


FIG. 7. Growth of the peak location of $f_D(y;t)$, $y_d(t)$, the mean domain size $\bar{y}(t)$, and the mean domain size over the samples of untwisted domains, $\bar{y}_+(t)$, and twisted domains, $\bar{y}_-(t)$, are, respectively, plotted with different kinds of lines. The correspondence between the kinds of lines and the quantities is indicated within the figure.

and retained in a large size region by subsequent annihilation events, collapses away from the side of the small size region.

The results in this section also suggest that in the 1D anisotropic XY-spin system, the DSDF changes its property from a scaling form to a solitonlike translational motion at a certain critical strength of anisotropy ($\gamma = 1/3$), as the strength of anisotropy diminishes.

Figure 7 shows the temporal behavior of some characteristic sizes: the growth of the peak location of $f_D(y;t)$, that of the mean domain size averaged over all domains, $\bar{y}(t)$, and that of the partially averaged sizes over the untwisted domains, $\bar{y}_+(t)$, and the twisted domains, $\bar{y}_-(t)$, are respectively plotted against time. These clearly indicate the logarithmic time dependence $\sim C \ln t$, where the coefficient C for each quantity is classified by two characteristic numbers as $y_d(t), \bar{y}_-(t), \bar{y}_-(t) \sim 0.93 \ln t$ and $\bar{y}_+(t) \sim 1.92 \ln t$. There is a notable difference between $\bar{y}_+(t)$ and $\bar{y}_-(t)$, being expressed as $\bar{y}_-(t) \approx y_d(t)$ and $\bar{y}_+(t) \approx 2.0 y_d(t)$. The former relation on $\bar{y}_-(t)$ implies that the growth of the mean size for the twisted domains is governed by the motion of the peak location of $f^<(y,-1;t)$. The latter relation can be intuitively explained as follows. Revisiting the above-mentioned argument for the creation of the untwisted domains, $Q=1$, in the small size region, the three consecutive domains with their arrangement of twistness $(-1,1,-1)$ dominate the creation of untwisted domains rather than that with (1,1,1) in the late stage. Hence, we can roughly estimate the resultant size of domains with $Q=1$ as $\sim y_d(t) + y_c + y_d(t) \sim 2y_d(t)$. Again this implies that the domain size statistics are governed by the dynamics of twisted domains.

IV. MASTER EQUATION

In this section, we formulate the master equation for the DSDF. In Sec. IV A, we introduce the n -body distribution function, and apply some simplifications for further develop-

ment, where some of those procedures are the same as used in the studies by NK [10,11]. In Sec. IV B, we calculate the probability for the realization of a specified twistness arrangement for n -consecutive domains. In Sec. IV C, we derive a reduced master equation for single domain size distribution function. The detailed analysis of the single domain size distribution function will be done in Sec. V.

A. n -body distribution function

Let us consider the temporal evolution of the assembly of domains described by Eqs. (2.5) and (2.3) under the periodic boundary condition $y_{i+N(t)}=y_i$ and $Q_{i+N(t)}=Q_i$, and the initial condition $\{y_1, y_2, \dots, y_{N_0}\} \equiv \{y\}_1^{N_0}$ and $\{Q_1, Q_2, \dots, Q_{N_0}\} \equiv \{Q\}_1^{N_0}$. As shown in Sec. II, for a given initial condition, the system has the conserved quantity, the total winding number W , defined by Eq. (2.6). Hence, the final distribution function at $t=\infty$ is written as

$$f(y, Q; \infty) = \begin{cases} \delta(y-L/|W|) \delta_{Q, -1} & \text{for } |W| \neq 0 \\ \delta(y-L) \delta_{Q, -1} & \text{for } |W| = 0, \end{cases} \quad (4.1)$$

where L is the system size. This expression indicates dependence on the initial configuration through the quantity W . In the present study, we are concerned with the long term behavior of the DSDF without dependence on the initial configuration and system size, and assume that the temporal evolution of the DSDF is parametrized with only a single-length scale being independent of the initial conditions. As well as the dynamical scaling behavior of the Néel wall system, the solitonlike translational motion, $h(y-y_d(t))$, can be characterized with the single size $y_d(t)$. Pointing to both scaling and solitonlike behavior, hereafter, we use the term *single-length scale behavior*, which means that both DSDF show similarities of domain size distribution through the change of single-length scale. Let us assume that such single-length scale behavior is achieved by taking the average over the possible initial configurations for large N_0 and L systems, also followed by taking the limit $L \rightarrow \infty$ and $N_0 \rightarrow \infty$ with the constraint N_0/L being constant. In this limit the DSDF does not reach the final state (4.1) since $\langle L/|W| \rangle \rightarrow \infty [O(\sqrt{N_0})]$, and let us assume convergence to an unique DSDF in this limit without proof.

The probability density function (PDF) for the state variables $\{y\}_1^n$ and $\{Q\}_1^n$ is defined as

$$\begin{aligned} f_n(y_1, Q_1; \dots; y_n, Q_n; t) \\ \equiv f_n(\{y, Q\}_1^n; t) \\ = \left\langle \prod_{k=1}^n \delta(y_k - y_k(t)) \delta_{Q_k, Q_k(t)} \right\rangle, \end{aligned} \quad (4.2)$$

where the definition range of y_i ($i=1, \dots, n$) is restricted to $y_i \geq y_c$, and $\langle \dots \rangle$ indicates the average over the possible initial configurations with equal weight, which is formally written as

$$\langle \dots \rangle \equiv \lim_{N_0, L \rightarrow \infty} \sum_{\{Q\}_1^{N_0}} 2^{-N_0} \int_{y_c}^{\infty} d\{y\}_1^{N_0} \delta\left(\sum_{l=1}^n y_l - L\right) \dots, \quad (4.3)$$

with the constraint N_0/L being constant. For simplicity, we use the notations,

$$\sum_{\{Q\}_1^n} \equiv \sum_{Q_1} \sum_{Q_2} \dots \sum_{Q_n}, \quad (4.4)$$

$$\int_{y_c}^{\infty} d\{y\}_1^n \equiv \int_{y_c}^{\infty} dy_1 \int_{y_c}^{\infty} dy_2 \dots \int_{y_c}^{\infty} dy_n, \quad (4.5)$$

where \sum_{Q_k} denotes the summation over $Q_k = \pm 1$. On the notation in Eq. (4.2), when we need to emphasize specific variable(s), we represent the n -body PDF as

$$\begin{aligned} f_n(y_1, Q_1; \dots; y_k, Q_k; \dots; y_n, Q_n; t) \\ \equiv f_n(\{y, Q\}_1^{k-1}; y_k, Q_k; \{y, Q\}_{k+1}^n; t). \end{aligned} \quad (4.6)$$

The n - and $(n-1)$ -body functions satisfy the relation

$$\sum_{\{Q_n\}} \int_{y_c}^{\infty} dy_n f_n(\{y, Q\}_1^n; t) = f_{n-1}(\{y, Q\}_1^{n-1}; t), \quad (4.7)$$

and the normalization condition is

$$\sum_{\{Q_1^n\}} \int_{y_c}^{\infty} d\{y\}_1^n f_n(\{y, Q\}_1^n; t) = 1.$$

Although these relationships are not held for the finite N_0 system, they will be practically satisfied in a sufficiently large N_0 system.

The master equation for the n -body distribution function is provided in the form

$$\begin{aligned} \frac{\partial}{\partial t} f_n(\{y, Q\}_1^n; t) = - \sum_{k=1}^n \frac{\partial}{\partial y_k} J_n^k(\{y, Q\}_1^n; t) \\ + \sum_{k=1}^n K_n^k(\{y, Q\}_1^n; t). \end{aligned} \quad (4.8)$$

Here, the term $J_n^k(\{y, Q\}_1^n; t)$ represents the k th component of the probability density flux in the space of n -consecutive variables $\{y, Q\}_1^n$, whose trajectory in the phase space is generated by Eq. (2.5). The term $K_n^k(\{y, Q\}_1^n; t)$ concerns the annihilation process (2.3), and means the production rate of the n -consecutive domains through the annihilation of the k th domain. Those expressions are given as

$$\begin{aligned} J_n^k(\{y, Q\}_1^n; t) \\ = \sum_{Q_0, Q_{n+1}} \int_{y_c}^{\infty} d\{y_0, y_{n+1}\} \\ \times v(y_{k-1}, Q_{k-1}; y_k, Q_k; y_{k+1}, Q_{k+1}) \\ \times f_{n+2}(\{y, Q\}_0^{n+1}; t), \end{aligned} \quad (4.9)$$

$$\begin{aligned}
& K_n^k(\{y, Q\}_1^n; t) \\
&= - \sum_{Q'Q''} \int_{y_c}^{\infty} d\{y', y''\} \delta_{Q_k, Q'} \delta_{Q'', Q'} \delta(y' + y_c + y'' - y_k) \\
&\quad \times v(y', Q'; y_c, 1; y'', Q'') \\
&\quad \times f_{n+2}(\{y, Q\}_1^{k-1}; y', Q'; y_c, 1; y'', Q''; \{y, Q\}_{k+1}^n; t),
\end{aligned} \tag{4.10}$$

where

$$\begin{aligned}
& v(y_{i-1}, Q_{i-1}; y_i, Q_i; y_{i+1}, Q_{i+1}) \\
&= Q_{i+1} e^{-y_{i+1}} + Q_{i-1} e^{-y_{i-1}} - 2Q_i e^{-y_i}
\end{aligned} \tag{4.11}$$

and $\int_{y_c}^{\infty} d\{x, y\} \equiv \int_{y_c}^{\infty} dx \int_{y_c}^{\infty} dy$. The boundary conditions for the n -body function are given as

$$\begin{aligned}
& f_n(\{y, Q\}_1^{k-1}; y_c, -1; \{y, Q\}_{k+1}^n; t) = 0, \\
& f_n(\{y, Q\}_1^{k-1}; y_c, 1; \{y, Q\}_{k+1}^n; t) \neq 0, \\
& f_n(\{y, Q\}_1^{k-1}; \infty, Q_k; \{y, Q\}_{k+1}^n; t) = 0,
\end{aligned} \tag{4.12}$$

for any k th domain ($1 \leq k \leq n$). The first condition is due to the repulsive nature of the motion of neighboring domain walls with $Q = -1$, Eq. (2.4), and the second reflects that the probability density flux for untwisted domains does not vanish at the boundary $y = y_c$ due to the presence of the annihilation process.

We can reduce Eq. (4.10) by two approximations into a more simplified form. (i) The annihilation speed $-v(y', Q'; y_c, 1; y'', Q'')$ is always positive for $y', y'' > y_c$, and its main part is dominated by the term $2e^{-y_c}$, the speed of solely collapsing domain. Hence, this allows us the simplification

$$v(y', Q'; y_c, 1; y'', Q'') \approx -2e^{-y_c}. \tag{4.13}$$

(ii) The correlation effect among three consecutive domain sizes, (y_{k-1}, y_c, y_{k+1}) , just before an annihilation event in which the middle of three domains collapses, does not significantly remain after the event. This allows the following approximation:

$$\begin{aligned}
& f_n(\{y, Q\}_1^{k-1}; y_c, Q_k; \{y, Q\}_{k+1}^n; t) \\
&\approx f_1(y_c, 1; t) f_{k-1}(\{y, Q\}_1^{k-1}; t) f_{n-k}(\{y, Q\}_{k+1}^n; t) \delta_{Q_k, 1},
\end{aligned} \tag{4.14}$$

for the k th collapsing domain ($1 \leq k \leq n$). This assumption regards the motion of the domains just before reaching the cutoff size as almost independent of the influence of the adjacent domains. Based on these approximations, Eq. (4.10) becomes

$$\begin{aligned}
& K_n^k(\{y, Q\}_1^n; t) \\
&\approx 2e^{-y_c} f_1(y_c, 1; t) \sum_{Q'Q''} \int_{y_c}^{\infty} d\{y', y''\} \delta_{Q_k, Q'} \delta_{Q'', Q'} \\
&\quad \times \delta(y' + y_c + y'' - y_k) f_k(\{y, Q\}_1^{k-1}; y', Q'; t) \\
&\quad \times f_{n-k+1}(y'', Q''; \{y, Q\}_{k+1}^n; t).
\end{aligned} \tag{4.15}$$

Collecting these results, we get the starting Eq. (4.8) with Eqs. (4.9) and (4.15) for the analysis of the DSDF.

B. Realization probability for a specified twistness arrangement

This section deals with the realization probability for a specified twistness arrangement $\{Q\}_1^n$ at time t . The master equation for the realization probability $f_n(\{Q\}_1^n; t)$ is obtained by integrating variables $\{y_1, \dots, y_n\}$ on both sides of the master Eq. (4.8) with Eqs. (4.9) and (4.15):

$$\begin{aligned}
& \frac{\partial}{\partial \tau} f_n(\{Q\}_1^n; \tau) \\
&= - \sum_{k=1}^n f_{k-1}(\{Q\}_1^{k-1}; \tau) f_{n-k}(\{Q\}_{k+1}^n; \tau) \delta_{Q_k, 1} \\
&\quad + \sum_{k=1}^n \sum_{Q', Q''} \delta_{Q_k, Q'} \delta_{Q'', Q'} f_k(\{Q\}_1^{k-1}, Q'; \tau) \\
&\quad \times f_{n-k+1}(Q'', \{Q\}_{k+1}^n; \tau),
\end{aligned} \tag{4.16}$$

where the time variable t is changed into τ by using

$$\partial_t \tau = 2e^{-y_c} f(y_c, 1). \tag{4.17}$$

For the case $n = 1$, Eq. (4.16) gives

$$\begin{aligned}
& \partial_{\tau} f_1(1; \tau) = -1 + f_1^2(1; \tau) + f_1^2(-1; \tau), \\
& \partial_{\tau} f_1(-1; \tau) = 2f_1(1; \tau)f_1(-1; \tau),
\end{aligned} \tag{4.18}$$

with the normalization condition $f_1(1; \tau) + f_1(-1; \tau) = 1$. For the case of the symmetric initial condition $f_1(Q_1; 0) = 1/2$, which was used for the present numerical analysis, Eq. (4.18) has the solution

$$f_1(Q_1; \tau) = \frac{e^{-\tau Q_1}}{e^{\tau} + e^{-\tau}}. \tag{4.19}$$

This result indicates that the number of negative- (positive) Q domains monotonically increases (decreases), and also that $\langle Q \rangle = -\tanh(\tau)$.

The solution for a general n case can be obtained by recursive procedure presented in Appendix A. For the symmetric initial condition $f_n(\{Q\}_1^n; 0) = 1/2^n$, the general n th probability function is found to be

$$f_n(\{Q\}_1^n; \tau) = \frac{\exp\left(-\tau \sum_{i=1}^n Q_i\right)}{\sum_{\{Q\}_n} \exp\left(-\tau \sum_{i=1}^n Q_i\right)}. \quad (4.20)$$

This proof is shown in Appendix A. This result is the n -times product of the single realization probability. The numerical check of the result (4.19) is shown in the following section.

C. Single domain size distribution function

The single domain size distribution function $f_1(y, Q; t)$ is given by integrating the variables $\{y\}_2^n$ and $\{Q\}_2^n$ in Eq. (4.8) with Eqs. (4.9) and (4.15), i.e.,

$$\frac{\partial}{\partial t} f_1(y, Q; t) = -\frac{\partial}{\partial y} J_1(y, Q; t) + K_1(y, Q; t), \quad (4.21)$$

where

$$\begin{aligned} J_1(y, Q; t) &= \sum_{Q', Q''} \int_{y_c}^{\infty} d\{y', y''\} v(y', Q'; y, Q; y'', Q'') \\ &\quad \times f_3(y', Q'; y, Q; y'', Q''; t), \\ &= -2Qe^{-y} f_1(y, Q; t) \\ &\quad + 2 \sum_{Q'} \int_{y_c}^{\infty} dy' Q' e^{-y'} f_2(y', Q'; y, Q; t), \end{aligned} \quad (4.22)$$

$$\begin{aligned} K_1(y, Q; t) &= 2e^{-y} c f_1(y_c, 1; t) \sum_{Q', Q''} \int_{y_c}^{\infty} d\{y', y''\} \delta_{Q, Q' Q''} \\ &\quad \times \delta(y' + y_c + y'' - y) \\ &\quad \times f_1(y', Q'; t) f_1(y'', Q''; t). \end{aligned} \quad (4.23)$$

By using this equation, the evolution of the mean domain size, $\bar{y}(t) = \sum_Q \int_{y_c}^{\infty} dy y f_1(y, Q; t)$, is estimated as

$$\begin{aligned} \dot{\bar{y}}(t) &\simeq 4e^{-y_c} c f_1(y_c, 1; t) \bar{y}(t) + 2y_c \langle Q e^{-y} \rangle f_1(y_c, 1; t) \\ &\simeq 4e^{-y_c} c f_1(y_c, 1; t) \bar{y}(t), \end{aligned} \quad (4.24)$$

where the second term in the first line is neglected since $e^{-y_c} \gg |\langle Q e^{-y} \rangle|$ for $\bar{y}(t) \gg y_c$. Eqs. (4.17) and (4.24) relate τ and $\bar{y}(t)$ as $\tau \simeq \frac{1}{2} \ln[\bar{y}(t)/\bar{y}(0)]$. In term of $\bar{y}(t)$, Eq. (4.19) reads

$$f_1(Q; \bar{y}(t)) = \begin{cases} \frac{\bar{y}(0)}{\bar{y}(t) + \bar{y}(0)} & (Q=1) \\ \frac{\bar{y}(t)}{\bar{y}(t) + \bar{y}(0)} & (Q=-1). \end{cases} \quad (4.25)$$

Figure 8 shows a comparison between the numerical result for the realization probability for the twistness of a single

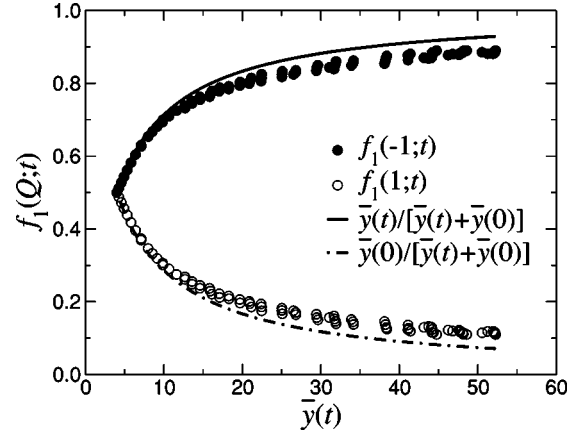


FIG. 8. Comparison between the numerical result for the realization probability for the twistness of a single domain and an analytical one, Eq. (4.25). Horizontal and vertical axes, respectively, indicate the average domain size and $f_1(Q; \bar{y}(t))$. Filled ($Q = -1$) and empty ($Q = 1$) circles correspond to the numerical results. Solid ($Q = -1$) and broken ($Q = 1$) lines represent Eq. (4.25) with $\bar{y}(0) = 4.0$.

domain and the analytical result Eq. (4.25) with $\bar{y}(0) = 4.0$, which is fixed over the present numerical calculations. When $\bar{y}(0)$ was treated as a fitting parameter, the best fitting value for $\bar{y}(0)$ by nonlinear curve fitting, was about 4.7. From these results, we can confirm that both results are in good agreement.

V. ANALYSIS OF DSDF FOR SINGLE DOMAIN

First, we carry out the a mean field analysis of the DSDF based on the dynamical scaling hypothesis. However, this approach will fail with an inconsistency with the hypothesis. As a result, this gives a proof for the absence of a scaling-type distribution in the Bloch wall regime, and indicates the necessity for incorporating the correlation effect between domain sizes. Next, we develop the analysis by incorporating the correlation between neighboring domain sizes, and show the qualitative solution for the solitonlike translational motion.

A. Mean field analysis

By using the factorization approximation, in which the joint PDF for two consecutive domains being replaced with

$$f_2(y_1, Q_1; y_2, Q_2; t) \simeq f_1(y_1, Q_1; t) f_1(y_2, Q_2; t), \quad (5.1)$$

and applying it into the drift term (4.22) in Eq. (4.21), we get

$$\begin{aligned} \frac{\partial}{\partial t} f(y, Q; t) &= -\frac{\partial}{\partial y} [2\mu(t) - 2Qe^{-y}] f(y, Q; t) \\ &\quad + \frac{\dot{\bar{y}}(t)}{\bar{y}(t)} K(y, Q; t), \end{aligned} \quad (5.2)$$

where $f(y, Q; t) \equiv f_1(y, Q; t)$ and $\mu(t) \equiv \langle Q e^{-y} \rangle$. From Eq. (4.25), $\langle Q \rangle < 0$ holds, then, $\mu(t)$ is negative except the early stage. The term $K(y, Q; t)$ in Eq. (5.2) is the rewrite of Eq. (4.23) by using Eq. (4.24), i.e., $K_1(y, Q; t) = [\dot{\bar{y}}(t)/\bar{y}(t)]K(y, Q; t)$.

Let us first consider the Eq. (5.2) without the reaction term $K(y, Q; t)$,

$$\frac{\partial}{\partial t} f^0(y, Q; t) = -\frac{\partial}{\partial y} V(y, Q; t) f^0(y, Q; t). \quad (5.3)$$

We have here defined the mean field force

$$V(y, Q; t) = -2e^{-y_D(t)} - 2Qe^{-y}, \quad (5.4)$$

where $\mu(t)$ in Eq. (5.2) is replaced with $-e^{-y_D(t)}$ by introducing the size $y_D(t)$ corresponding to the vanishing point of the mean field force for $Q = -1$, i.e., $V(y_D(t), -1; t) = 0$. It is expected that $y_D(t)$ is close to $y_d(t)$ [$y_d(t)$ is defined in Sec. III].

The solution for a given initial distribution $f^0(y, Q; 0)$ can be obtained by solving the equation of motion $\dot{y} = V(y, Q; t)$. Let $y(\eta, Q; t)$ be its solution trajectory at time t with the initial condition $y(\eta, Q; 0) = \eta$, then let us assume the form of $y(\eta, Q; t)$ as

$$y(\eta, Q; t) = \ln[e^{\eta - QB(t)}] - A(t), \quad (5.5)$$

where $A(t)$ and $B(t)$ must satisfy the equations $\dot{A}(t) = 2e^{-y_D(t)}$ and $\dot{B}(t) = 2e^{A(t)}$ with the initial conditions $A(0) = B(0) = 0$. The inverse of the solution (5.5), i.e., the trajectory starting with y at $t = 0$ and ending with η after the time t , becomes

$$\eta(y, Q; t) = \ln[QB(t) + e^{y+A(t)}]. \quad (5.6)$$

By using Eq. (5.6), the solution of Eq. (5.3) is written in the form

$$f^0(y, Q; t) = \begin{cases} \frac{1}{1+B(t)e^{-y-A(t)}} f^0(\eta(y, 1; t), 1; 0) \theta(y - y_c) & (Q=1) \\ \frac{1}{1-B(t)e^{-y-A(t)}} f^0(\eta(y, -1; t), -1; 0) \theta(y - y_c(t)) & (Q=-1), \end{cases} \quad (5.7)$$

with $y_c(t) = \ln[e^{y_c} + B(t)] - A(t)$.

Here, the technical details of Eq. (5.7) are as follows. The expressions for $A(t)$ and $B(t)$ are obtained by supposing the relation $A(t) = \alpha[y_D(t) - y_D(0)]$ with a constant $\alpha > 0$, so that it leads to the $\ln t$ -behavior for $y_D(t)$, i.e.,

$$y_D(t) = \ln\left[\frac{2}{\alpha}t + e^{y_D(0)}\right], \quad (5.8)$$

$$A(t) = \alpha(y_D(t) - y_D(0)) = \alpha \ln\left[1 + \frac{2}{\alpha}e^{-y_D(0)}t\right], \quad (5.9)$$

$$B(t) = \frac{\alpha e^{y_D(0)}}{1+\alpha} \left[\left(1 + \frac{2}{\alpha}e^{-y_D(0)}t\right)^{1+\alpha} - 1 \right] \\ = \frac{\alpha e^{y_D(0)}}{1+\alpha} [e^{(1+\alpha)\alpha A(t)} - 1]. \quad (5.10)$$

The step-function factors for $Q = \pm 1$ in Eq. (5.7) represent the definition ranges of y for the function $f^0(y, \pm 1; t)$, those are determined by the following argument. The ranges of the variables y and η are restricted to $y, \eta \geq y_c$. In addition to these, from Eq. (5.6), $\eta(y, Q; t) \geq \max[\ln[QB(t) + e^{y+A(t)}], y_c]$ must be also satisfied, where $\max[x, y]$ means the maximum of the set $\{x, y\}$. This yields

$$\eta \geq \begin{cases} \ln[B(t) + e^{y_c+A(t)}] & (Q=1) \\ y_c & (Q=-1). \end{cases} \quad (5.11)$$

Therefore, from Eq. (5.5), the regions for y are limited to $y \geq y_c$ ($Q=1$) and $y \geq y_c(t)$ ($Q=-1$) as shown in Eq. (5.7). For large $y_D(t)$, $y_c(t)$ is estimated as $y_c(t) \sim y_D(t) + \ln[\alpha/(1+\alpha)]$ from Eqs. (5.9) and (5.10).

In Eq. (5.7) the solution for $Q=1$ takes the asymptotic form

$$f^0(y, 1; t) \approx \begin{cases} f^0(y+A(t), 1; 0) & \text{for } y > y_c(t) \\ e^{y-y_c(t)} f^0(\ln B(t), 1; 0) & \text{for } y < y_c(t), \end{cases} \quad (5.12)$$

for the situation $y_c(t) \gg y_c$. The prefactor exhibits a step-function-like form, which exponentially decays toward the region $y < y_c(t)$ with its decay width of order one, and $y_c(t)$ is regarded as an effective cutoff size. The asymptotic form (5.12) indicates that the probability mass for untwisted domain sizes flows out of the effective region $y > y_c(t)$. Similarly, the solution for $Q=-1$ takes the form $f^0(y+A(t), -1; 0)$ for $y \geq y_c(t)$ and $B(t)e^{-y_c} f^0(y_c, -1; 0)$ at $y = y_c(t)$, where $B(t) \sim t^{1+\alpha}$. These forms indicate that the probability mass for the twisted domain sizes flows into the size $y = y_c(t)$ and accumulates. The present analysis follows the treatment in Ref. [10] for the Néel wall situation. However, the behavior shown here is quite different from that of

the Néel wall situation, in which the expression corresponding to $f^0(y+A(t),1;0)$ of the present case was like $f^0(y-A(t),1;0)$. The difference here is owing to the negative sign of $\mu(t)$ in Eq. (5.2), and it is also critical for the long term behavior of the DSDF between both systems.

Now, taking the reaction term $K(y,Q;t)$ into account, we assume the form of the solution for Eq. (5.2) as

$$f(y,Q;t) = \frac{\partial \eta(y,Q;t)}{\partial y} G(\eta(y,Q;t),Q;t) \quad (5.13)$$

with a function G , which is a generalization of Eq. (5.7). Substituting this into Eq. (5.2), we obtain

$$\frac{\partial}{\partial t} G(\eta,Q;t) = \frac{\dot{y}(t)}{\bar{y}(t)} \frac{\partial y(\eta,Q;t)}{\partial \eta} K(y(\eta,Q;t),Q;t), \quad (5.14)$$

where η is changed to be an independent variable with the map (5.5) : $\eta \rightarrow y$, and $K(y(\eta,Q;t),Q;t)$ becomes

$$\begin{aligned} & \frac{1}{2} \sum_{Q'} \int_{\eta_c^{Q'}(t)}^{\infty} d\eta' \int_{\eta_c^{QQ'}(t)}^{\infty} d\eta'' \delta(y(\eta',Q';t)+y_c \\ & + y(\eta'',QQ';t) - y(\eta,Q;t)) \\ & \times G(\eta',Q';t) G(\eta'',QQ';t), \end{aligned} \quad (5.15)$$

where the lower cutoff of the integral is denoted as $\eta_c^Q(t)$. In the present treatment, $\eta_c^Q(t) = \eta(y_c, Q; t)$ [the definition range of η is shown in Eq. (5.11)]. However, that value has been obtained free of the annihilation process and correlation effects, thus it may differ from values in more advanced treatments.

With the Laplace transformation

$$\tilde{G}(p,Q;t) = \int_{\eta_c^Q(t)}^{\infty} d\eta e^{-p\eta} G(\eta,Q;t), \quad (5.16)$$

Eq. (5.14) is rewritten as

$$\begin{aligned} & \frac{\partial}{\partial t} \tilde{G}(p,Q;t) + \dot{\eta}_c^Q(t) e^{-p\eta_c^Q(t)} G(\eta_c^Q(t),Q;t) \\ & = \frac{1}{2} \frac{\dot{y}(t)}{\bar{y}(t)} \sum_{Q'} \int_{\eta_c^{Q'}(t)}^{\infty} d\eta' \int_{\eta_c^{QQ'}(t)}^{\infty} d\eta'' \\ & \times e^{-pY(\eta',Q';\eta'',QQ';t)} G(\eta',Q';t) G(\eta'',QQ';t), \end{aligned} \quad (5.17)$$

where

$$\begin{aligned} Y(\eta',Q';\eta'',QQ';t) & = \eta[y(\eta',Q';t)+y_c+y(\eta'',QQ';t),Q;t] \\ & = \eta' + \eta'' - A(t) + \Delta Y(\eta',Q';\eta'',QQ';t), \end{aligned} \quad (5.18)$$

$$\begin{aligned} e^{\Delta Y(\eta',Q';\eta'',QQ';t)} & = e^{y_c} [1 - Q' B(e^{-\eta'} + Q e^{-\eta''}) \\ & + QB(B + e^{A-y_c}) e^{-\eta' - \eta''}]. \end{aligned} \quad (5.19)$$

The term ΔY in Eq. (5.18) is negligible for $\eta', \eta'' \gg \eta(y_c, 1; t)$, but it can be relevant around the lower cutoff of the integral. For $Q = -1$ and $Q' = 1$, at the cutoffs $\eta' = \eta(y_c, 1; t)$ and $\eta'' = \eta(y_c, -1; t) = y_c$, the factor (5.19) is estimated as

$$e^{y_c} \left[1 - \frac{B}{B + e^{A+y_c}} + B e^{-y_c} - \frac{B(B + e^{A-y_c}) e^{-y_c}}{B + e^{A+y_c}} \right] \sim 0,$$

for large t . Similarly, for $Q = 1$ and $Q' = 1$, at the cutoff $\eta', \eta'' = \eta(y_c, 1; t)$ the factor (5.19) vanishes, and for $Q = 1$ and $Q' = -1$, at the cutoff $\eta', \eta'' = y_c$ the factor (5.19) diverges for large t . Now, we are concerned with the problem whether the function $G(\eta, Q; t)$ is written in a dynamical scaling form on η with a length scale parameter or not. In order to examine that, we discuss Eq. (5.14) or Eq. (5.17) under the assumption that Eq. (5.14) has the scaling range in which $G(\eta, Q; t)$ obeys the dynamical scaling behavior as written in the form $G(\eta, Q; t) \sim g[\eta/\bar{\eta}^Q(t), Q; t]/\bar{\eta}^Q(t)$ with a scaling length $\bar{\eta}^Q(t)$. For this point of view, the contribution from the factor (5.19) presented above already breaks the scaling behavior since the terms in Eq. (5.19) are not written in scaling form. For this situation, in order to extract the scaling region, we introduce an effective cutoff as written in $\eta_c^Q(t) \propto A(t)$ [$\propto \bar{\eta}^Q(t)$] so that the factor (5.19) can be regarded to have an order of unity. By replacing the cutoff, we put $G(\eta, Q; t)$ as $G(\eta, Q; t) = G'(\eta, Q; t) \theta(\eta - \eta_c^Q(t))$, and ΔY as $\Delta Y \sim 0$. The remaining contribution from the term (5.19) can be considered to be of a comparable order to the correlation effect neglected in the factorization approximation for the drift term (4.22), i.e., expanding Eq. (5.18) as

$$\begin{aligned} e^{-pY(\eta',Q';\eta'',QQ';t)} & = e^{-p[\eta' + \eta'' - A(t) + y_c]} \\ & \times [1 + C_1 p + C_2 p^2 + \dots], \end{aligned} \quad (5.20)$$

with the expansion coefficients $C_k \equiv C_k(\eta', Q'; \eta'', QQ'; t)$ ($k = 1, 2, \dots$), where y_c in the prefactor is negligible for $A(t)$. The terms higher than the p^0 th order can be regarded as concerning correlation effects relevant to the nonscaling region $\eta(y_c, Q; t) < \eta < \eta_c^Q(t)$.

Discarding the terms obviously breaking the dynamical scaling form, Eq. (5.17) becomes

$$\begin{aligned} & \frac{\partial}{\partial t} \tilde{G}(p,Q;t) + \dot{\eta}_c^Q(t) e^{-p\eta_c^Q(t)} G(\eta_c^Q(t),Q;t) \\ & = \frac{1}{2} \frac{\dot{y}(t)}{\bar{y}(t)} e^{pA(t)} \sum_{Q'} \tilde{G}(p,Q';t) \tilde{G}(p,QQ';t). \end{aligned} \quad (5.21)$$

Since, for $p = 0$, Eq. (5.21) must be consistent with Eq. (4.18), in which the time scales τ and t are connected via Eqs. (4.17) and (4.24), we have

$$G(\eta_c^Q(t), Q; t) = \left[\frac{\eta_c^1 \dot{y}}{\eta_c^1 \bar{y}} \right] \frac{1}{2 \eta_c^1(t)} \delta_{Q,1} = \frac{1}{2 \eta_c^1(t)} \delta_{Q,1}, \quad (5.22)$$

where the prefactor in the second expression is assumed to quickly saturate to 1. With the scale transformations,

$$\eta_c^1 p = s, \quad \partial_t \tau = \frac{\dot{\eta}_c^1}{2 \eta_c^1}, \quad \tilde{G}(p, Q; t) = \tilde{g}(\eta_c^1 p, Q; \tau), \quad (5.23)$$

Eq. (5.21) is rewritten as

$$\begin{aligned} \frac{\partial}{\partial \tau} \tilde{g}(s, Q; \tau) + 2s \frac{\partial}{\partial s} \tilde{g}(s, Q; \tau) + e^{-s} \delta_{Q,1} \\ = e^{\beta s} \sum_{Q'} \tilde{g}(s, Q'; \tau) \tilde{g}(s, Q Q'; \tau), \end{aligned} \quad (5.24)$$

where the parameter β is defined with the limit $A/\eta_c^1 \rightarrow \beta$ (>0), or $\eta_c^1 \sim \alpha/\beta y_D(t)$, for large t .

To examine whether Eq. (5.24) has a scaling solution, let us see the behavior of the moment hierarchical equations defined for the coefficients of the expansion $\tilde{g}(s, Q; \tau) = \sum_{n=0}^{\infty} M_n^Q s^n$, where $M_n^Q \equiv (-1)^n \langle [\eta/\eta_c^1(t)]^n \rangle_Q / n!$ concerns the n th moment of scaled domain size $\eta/\eta_c^1(t)$. $M_0^Q \equiv M_0^Q(\tau)$ is the normalization factor already obtained as $M_0^Q = f(Q; \tau)$ at Eq. (4.19). The equations for the first moment M_1^Q are obtained for the s^1 -order expansion of Eq. (5.24). The calculation of M_1^Q is shown in Appendix B. From the result in Appendix B, it is found that $M_1^Q \sim (1 + \beta)\tau/2$ for large τ . Therefore, the first moment, i.e., the mean of scaled domain size

$$\langle \eta/\eta_c^1(t) \rangle_Q = -M_1^Q \sim -\frac{1 + \beta}{2} \tau \quad (5.25)$$

diverges to $-\infty$ because of $\beta > 0$. The restriction $\beta > 0$ originates from the direction of the mean field force $V(y, 1; t)$ always being negative. This result is inconsistent with the dynamical scaling assumption, which requires $\langle \eta/\eta_c^1(t) \rangle_Q$ to be constant, hence, we can conclude that the long term behavior of the DSDF cannot be described as a scaling-type distribution.

B. Correlation effect

The argument in the preceding section suggests that the correlation effect omitted in the factorization approximation is crucial for the description of the DSDF. Based on this fact, the following treatment makes the joint PDF for two consecutive domains expand as

$$\begin{aligned} f_2(y_1, Q_1; y_2, Q_2; t) = f(y_1, Q_1; t) f(y_2, Q_2; t) \\ + G_2(y_1, Q_1; y_2, Q_2; t). \end{aligned} \quad (5.26)$$

This progresses the factorization approximation with the function $G_2(y_1, Q_1; y_2, Q_2; t) (\equiv G_2)$. The explicit form of G_2 is given in Appendix C by omitting Q variables, there we introduce the identities extracting the correlation effect from the joint PDF for two variables based on the characteristic function theory. Corresponding to Eq. (C11) in Appendix C, G_2 is written as

$$\begin{aligned} G_2 = \frac{\partial^2}{\partial y_1 \partial y_2} \int_{y_c}^{\infty} d\{y'_1, y'_2\} C_2(y_1 - y'_1, Q_1; y_2 - y'_2, Q_2; t) \\ \times f(y'_1, Q_1; t) f(y'_2, Q_2; t), \end{aligned} \quad (5.27)$$

where $C_2(Y_1, Q_1; Y_2, Q_2; t) (\equiv C_2)$ corresponds to Eq. (C12) in Appendix C. And according to Eq. (C15) in Appendix C, C_2 satisfies the sum rule

$$\begin{aligned} \int_0^{\infty} d\{Y_1, Y_2\} C(Y_1, Q_1; Y_2, Q_2; t) \\ = \langle y_1 y_2 \rangle_{Q_1, Q_2} - \langle y_1 \rangle_{Q_1, Q_2} \langle y_2 \rangle_{Q_1, Q_2} \\ \equiv D_{Q_1, Q_2}(t), \end{aligned} \quad (5.28)$$

where $\langle \dots \rangle_{Q_1, Q_2}$ denotes the integral

$$\langle \dots \rangle_{Q_1, Q_2} \equiv \int_{-\infty}^{\infty} d\{y_1, y_2\} f_2(y_1, Q_1; y_2, Q_2; t) (\dots), \quad (5.29)$$

namely, the quantity $D_{Q_1, Q_2}(t)$ is the covariance that characterizes the correlation between neighboring domains those twistness is specified by $\{Q_1, Q_2\}$.

So far, Eq. (5.26) and the associated equations are nothing but the rewriting of the original two-body PDF, for further development, other independent information for C_2 is needed. In the present analysis, we assume that the function $C_2(Y_1, Q_1; Y_2, Q_2; t)$ quickly decays for large $Y_{1,2} (>0)$, which satisfies the sum rule (5.28), and meets the form of Eq. (C13). Then, as an extreme case of such a function, we apply

$$C_2 \approx D_{Q_1, Q_2}(t) \delta(Y_1 - \epsilon) \delta(Y_2 - \epsilon) \theta(Y_1) \theta(Y_2), \quad (5.30)$$

where ϵ is a small positive number, for which we will take the limit $\epsilon \rightarrow +0$. Although there are other choices of C_2 , e.g.,

$$C_2 \approx \frac{D_{Q_1, Q_2}(t)}{D_{Q_1} D_{Q_2}} e^{-Y_1/D_{Q_1} - Y_2/D_{Q_2}} \theta(Y_1) \theta(Y_2), \quad (5.31)$$

with finite widths, D_{Q_1} and D_{Q_2} , though we will not use them here. C_2 given by Eq. (5.30) is the most simplified treatment taking the correlation into account.

Substituting Eq. (5.30) to Eq. (5.27), we obtain

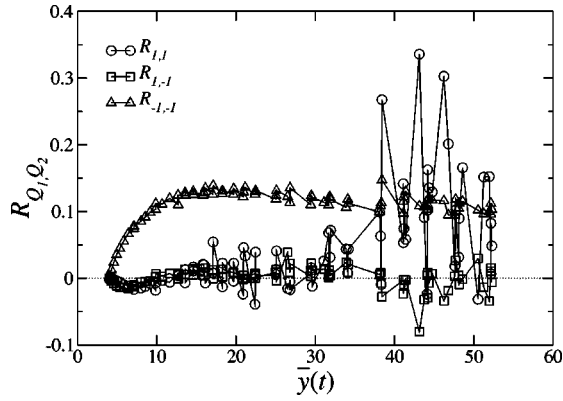


FIG. 9. Temporal change of the correlation coefficients $R_{1,1}$, $R_{1,-1}$, and $R_{-1,-1}$. The vertical and horizontal axes indicate the value of R_{Q_1, Q_2} and the mean domain size $\bar{y}(t)$, respectively. The correspondence between each of R_{Q_1, Q_2} and kind of symbol is indicated within the figure.

$$G_2 = D_{Q_1, Q_2}(t) \frac{\partial^2}{\partial y_1 \partial y_2} \theta(y_1 - y_c - \epsilon) \theta(y_2 - y_c - \epsilon) \times f(y_1, Q_1) f(y_2, Q_2). \quad (5.32)$$

Then the probability density flux (4.22) is replaced with

$$J_1(y, Q; t) = V(y, Q; t) f(y, Q; t) - \nu_Q(t) \frac{\partial}{\partial y} f(y, Q; t), \quad (5.33)$$

where

$$\nu_Q(t) \equiv - \sum_{Q'} \int_{y_c}^{\infty} dy' D_{Q, Q'}(t) Q' e^{-y'} f(y', Q'; t). \quad (5.34)$$

At the appropriate step in the calculation to Eq. (5.33), we have taken the limit $\epsilon \rightarrow +0$.

If the coefficient (5.34) does not take a well defined value, our approximation will be meaningless, or if it takes negative value, it may indicate the need of more higher order moments. Figure 9 shows the temporal change of the correlation coefficient

$$R_{Q_1, Q_2} \equiv \frac{\langle y_1 y_2 \rangle_{Q_1, Q_2} - \langle y_1 \rangle_{Q_1, Q_2} \langle y_2 \rangle_{Q_1, Q_2}}{\sqrt{\langle \delta y_1^2 \rangle_{Q_1, Q_2} \langle \delta y_2^2 \rangle_{Q_1, Q_2}}} = \frac{D_{Q_1, Q_2}(t)}{\langle \delta y_1^2 \rangle_{Q_1, Q_2}}, \quad (5.35)$$

where $\delta y_{1,2} \equiv y_{1,2} - \langle y_{1,2} \rangle_{Q_1, Q_2}$. In the figure the quantity $R_{-1,-1}$ exhibits a well defined behavior, i.e., it smoothly changes and saturates to a constant value within the range 0.10–0.12. However, the data points for $R_{1,1}$ and $R_{1,-1}$ exhibit a scatter behavior, the vibration around the zero axis. The main cause of the scatter behavior is considered to be a finite size effect because of the monotonic decreasing of the number of domains. From these results we can regard the quantity $R_{-1,-1}$ as positive, and in effect put $R_{1,1}$ and $R_{1,-1}$ to zero. Although the mean of $R_{1,1}$ shows a tendency to shift

to the positive side, we ignore it; that is considered to be the second effect propagated from the original correlation among negative- Q pairs of domains. This observation leads to

$$\nu_Q(t) \approx \begin{cases} 0 & (Q=1) \\ \int_{y_c}^{\infty} dy' D_{-1,-1}(t) e^{-y'} f(y', -1; t) & (Q=-1). \end{cases} \quad (5.36)$$

Substituting Eqs. (5.33) and (5.36) into Eq. (4.21), we get

$$\frac{\partial}{\partial t} f^1(y, 1; t) \approx - \frac{\partial}{\partial y} V(y, 1; t) f^1(y, 1; t) + K_1(y, 1; t), \quad (5.37)$$

$$\begin{aligned} \frac{\partial}{\partial t} f^1(y, -1; t) \approx & - \frac{\partial}{\partial y} \left[V(y, -1; t) - \nu_{-1}(t) \frac{\partial}{\partial y} \right] f^1(y, -1; t) \\ & + K_1(y, -1; t). \end{aligned} \quad (5.38)$$

In a similar sense to the expression (3.5) in Sec. III, we anticipate the DSDF to be written in the form

$$f^1(y, Q; t) = f^<(y, Q; t) + g(y; t) + (\text{interference terms}),$$

where $f^<(y, Q; t)$ and $g(y; t)$ corresponds to the DSDF for the small and large size region, and the interference terms consist of various combinations of them.

As shown in the numerical simulation, the single-length scale behavior is described as a solitonlike motion. Now, that behavior corresponds to the term of $f^<(y, -1; t)$, namely, $f^<(y, -1; t)$ has a sharp peak around the size $y = y_d(t)$ [$\sim y_D(t)$], which corresponds to the average size of the clusters that consist of domain sizes dispersed in a narrow range around that size. Hence the dynamics of the DSDF will be reduced to the dynamics limited in the narrow range, and we focus our attention to the behavior of $f^<(y, -1; t)$. The dispersion of domain sizes can be regarded as the result of the annihilation of domains, i.e., the role of the annihilation is nothing but to prevents all domain sizes from being condensed into one domain size $y_d(t)$ together with driving the domain size growth. We can expect that the DSDF for $Q=1$ is slaved to $f^<(y, -1; t)$ around the region $y \sim y_d(t)$ as discussed in Sec. III.

From the numerical results, we postulate $f^1(y, -1; t)$ can be written as

$$f^1(y, -1; t) \approx H(t) h(y - y_D(t); t), \quad (5.39)$$

with a quasistationary function h , where the coefficient $H(t)$ can be regarded as the order parameter reflecting the broken symmetry of chirality $\langle Q \rangle \neq 0$. Figure 5(a) shows that $H(t)$ grows from $H(0) \approx 0$ and saturates to a constant value, and suggests that $H(t)$ can be expressed in terms of $f(-1; t) - f(1; t) = -\langle Q \rangle$.

Substituting Eq. (5.39) into Eq. (5.38), we get

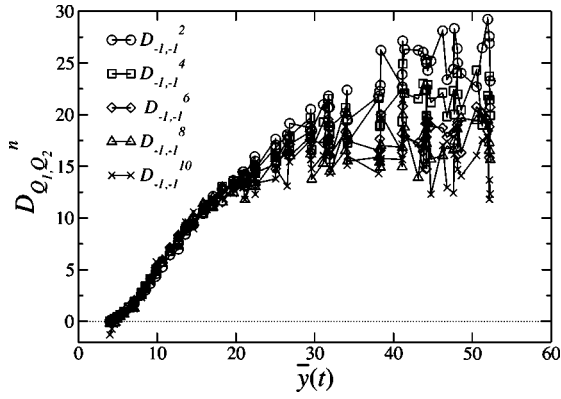


FIG. 10. The temporal change of the covariance $D_{-1,-1}^n(t)$ ($n = 2, \dots, 10$) is defined by Eq. (5.45). The vertical and horizontal axes, respectively, indicate the value of $D_{-1,-1}^n(t)$ and the mean domain size $\bar{y}(t)$. The correspondence between each number n and the kind of symbol is indicated within the figure.

$$\frac{\partial}{\partial s} h(z; s) \simeq -\frac{\partial}{\partial z} \left[\left[e^{-z} - a(s) \right] - b(s) \frac{\partial}{\partial z} \right] h(z; s) + \Delta K_1(z, -1; t) \Big|_{t=t(s)}, \quad (5.40)$$

where $z \equiv y - y_D(t)$ and the new time variable s is introduced with the transformation $\dot{s} = 2e^{-y_D(t)}$. The coefficients and the term $\Delta K_1(z, -1; t) (\equiv \Delta K_1)$ in Eq. (5.40) are defined as

$$a(s) = 1 + \frac{1}{2} e^{y_D(t)} \dot{y}_D(t) \Big|_{t=t(s)}, \quad (5.41)$$

$$b(s) = \frac{1}{2} v_{-1}(t) e^{y_D(t)} \Big|_{t=t(s)}, \quad (5.42)$$

$$\Delta K_1 = -\frac{e^{y_D(t)}}{2H(t)} \{ \dot{H}(t) h(z; t) - K_1[z + y_D(t), -1; t] \}. \quad (5.43)$$

For $a(s)$, $b(s)$, and ΔK_1 , we estimate their time dependency as follows. For $a(s)$, from the numerical result $y_d(t) \sim \ln t$ [this also implies $y_D(t) \sim \ln t$], it can be regarded to be a constant for a sufficiently large t . Next, from the requirement for $h(z; s)$ being quasistationary, we should choose $H(t)$ so as to satisfy $\int_{y_c}^{\infty} dy \Delta K_1 \sim 0$. By using Eqs. (4.23) and (4.24), this makes $\dot{H}(t) \sim f(-1; t) f(1; t) \dot{\bar{y}}(t) / \bar{y}(t)$, thereby we find $H(t) \propto [f(-1; t) - f(1; t)]$ with Eq. (4.18) [note that $H(t) \propto f(-1; t)$ for a sufficiently large t and $H(0) \sim 0$ is the desired initial condition for $H(t)$]. The order estimation of Eq. (5.43) gives $\Delta K_1 \sim e^{y_D(t)} f(1; t) \dot{\bar{y}}(t) / \bar{y}(t)$. This leads to $\Delta K_1 \sim \bar{y}(t)^{-2}$ by means of $\dot{\bar{y}}(t) \sim e^{-y_D(t)}$ and $f_1(1; \bar{y}(t)) \sim \bar{y}(t)^{-1}$ [see Eq. (4.25)]. Accordingly, hereafter, we drop the term ΔK_1 from Eq. (5.40), since it becomes negligible in comparison with the other terms in the order unity. The remaining parameter $b(s)$ is written as

$$b(s) \simeq \frac{H(t(s))}{2} D_{-1,-1}(t(s)) \int_{-y_D(t(s))}^{\infty} dz' e^{-z'} h(z'; s), \quad (5.44)$$

from Eqs. (5.42) and (5.36). The factor $H(t)$ and the integral value of the last factor, respectively, saturate to certain constant values with an order unity for large $y_D(t)$. In the present approach, as $D_{-1,-1}(t)$ can not be explicitly expressed with known quantities, we then estimate the time dependency of $D_{-1,-1}(t)$ numerically as in the following paragraph.

Figure 10 shows the temporal behavior of the quantity

$$D_{-1,-1}^n(t) \equiv \langle y_1 y_2 \rangle_{\{-1, \dots, -1\}^n} - \langle y_1 \rangle_{\{-1, \dots, -1\}^n} \langle y_2 \rangle_{\{-1, \dots, -1\}^n}, \quad (5.45)$$

for $n = 2, \dots, 10$, where $\langle \dots \rangle_{\{-1, \dots, -1\}^n}$ is the average taken over the ensembles of n -consecutive domains whose twistness are all $Q = -1$, and in which the neighboring domains numbered as 1 and 2 are located at the center of the array. In particular, the case $n = 2$ is identical to $D_{-1,-1}(t)$. It is found that $D_{-1,-1}^n(t)$ increases in the course of time over all n , and its magnitude for larger n takes smaller values at the same time. Here, it is important that as n is large the temporal behavior of $D_{-1,-1}^n(t)$ indicates a tendency to saturate to a constant value [although $D_{-1,-1}^2(t)$ does not clearly reach a constant value, $D_{-1,-1}^{10}(t)$ though clearly reaches]. This agrees with an observation that the quantity $D_{-1,-1}^n(t)$ for a large n extracts the correlation between neighboring domain sizes inside of clusters in which domain sizes are ordered with sizes around $y_d(y)$, while $D_{-1,-1}^n(t)$ for smaller n is more influenced by the disordered domain sizes outside of the clusters. From this observation, we assume that $D_{-1,-1}(t)$ consists of two parts as $D_{-1,-1}(t) = D_{-1,-1}^{\infty} + \delta D_{-1,-1}(t)$ with the constant part $D_{-1,-1}^{\infty}$, the contribution from the ordered domain sizes, and $\delta D_{-1,-1}(t)$ diminishing in the course of time, the contribution from the disordered ones. According to this decomposition, we also assume $h(y - y_D(t); t)$ to be separable as

$$h(y - y_D(t); t) = h(y - y_D(t))^{\infty} + \delta h(y - y_D(t); t), \quad (5.46)$$

where the shape of the former function is stationary and the latter temporally diminishes. Similarly, from Eq. (5.44) and these assumptions, the coefficient $b(s)$ is also decomposed into a constant b^{∞} and another temporally diminishing part $\delta b(s)$ as $b(s) = b^{\infty} + \delta b(s)$. Substituting the expansion for $b(s)$ and Eq. (5.46) into Eq. (5.40), and collecting only the stationary terms, we get

$$\frac{\partial}{\partial s} h(z; s) \simeq -\frac{\partial}{\partial z} \left[(e^{-z} - a^{\infty}) - b^{\infty} \frac{\partial}{\partial z} \right] h(z; s), \quad (5.47)$$

where a^{∞} is the constant part of $a(s)$ in the limit $s \rightarrow \infty$. It is expected that the remaining temporally varying terms are comparable with the reaction term ΔK_1 . The form of Eq.

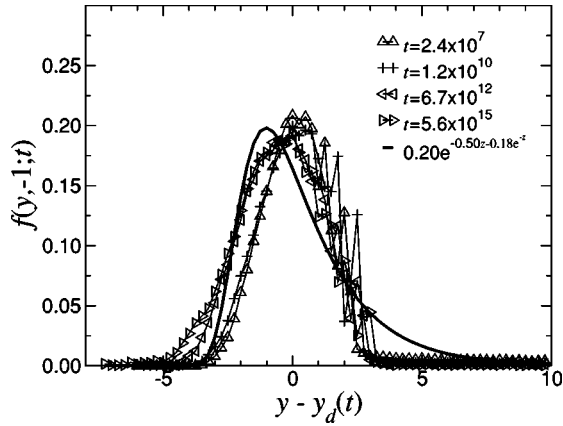


FIG. 11. Typical shape of Eq. (5.48) (solid line) and the numerical data for $f(y, -1; t)$ whose peak position is shifted to the origin. The parameters in Eq. (5.48) are chosen as $0.20 \exp[-0.50z - 0.18 \exp(-z)]$.

(5.47) is the Fokker-Planck equation with an exponentially decaying potential. The stationary solution of Eq. (5.47) is given by

$$h^\infty(z) \approx C \exp[-\{a^\infty z + \exp(-z)\}/b^\infty], \quad (5.48)$$

where C is a constant. More advanced treatment of Eq. (5.47) is found in Ref. [21].

Figure 11 shows a comparison between the numerical data and the typical shape of Eq. (5.48), $0.20 \exp[-0.50z - 0.18 \exp(-z)]$, whose parameters were obtained with a nonlinear curve fitting to the data for $t = 6.7 \times 10^{12}$. The difference between both results is relatively large for the region $z > 0$.

One reason why the difference arises is that there is non-stationary behavior in the numerical data, which has been eliminated in the analytical result. Another cause may lie in the truncation of higher order moments concerning the cor-

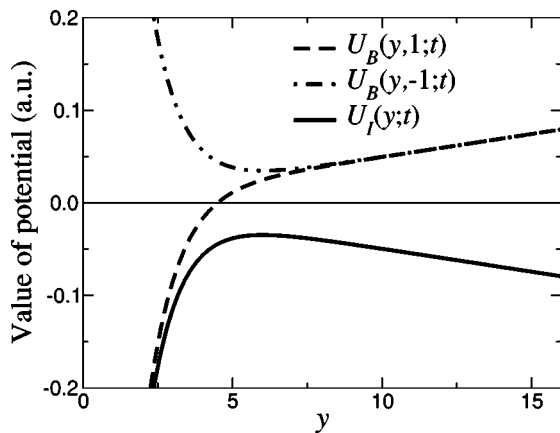


FIG. 12. Typical behaviors of the mean field potentials, $U_B(y, Q; t)$ [$Q = 1$ (-1) correspond to broken (doubly broken) line] and $U_I(y; t)$ (solid line). The vertical and horizontal axes indicate the values of the potentials (arbitrary unit) and y , respectively. For all these functions, $y_D(t)$ is set to be 6.0.

relation effect in the derivation of Eq. (5.33), since the more detailed shape of the DSDF is considered to be sensitive to higher order moments.

VI. DISCUSSION

In this section, we discuss the difference in the domain growth behaviors between the Néel and Bloch wall situations. Except for the detailed shape of the DSDF, the characteristics of the DSDF in the Bloch wall situation lie in the structure of the mean field force $V(y, Q; t)$ as defined by Eq. (5.4). In the Néel wall situation, from Eq. (1.3), the mean field force is obtained as

$$\dot{y} = 2e^{-y_D(t)} - 2e^{-y} \equiv V_I(y). \quad (6.1)$$

We can also define the potential functions from the force fields Eqs. (5.4) and (6.1) by integrating them on the variable y , i.e.,

$$U_B(y, Q; t) = 2e^{-y_D(t)}y - 2Qe^{-y}, \quad (6.2)$$

$$U_I(y; t) = -2e^{-y_D(t)}y - 2e^{-y}, \quad (6.3)$$

for the Bloch (U_B) and Néel (U_I) wall situations, respectively. The typical behaviors of these functions are shown in Fig. 12. The potential $U_B(y, -1; t)$ has a minimum at $y = y_D(t)$, and $U_B(y, 1; t)$ has an attractive point at the cutoff size $y = y_c$, where domain sizes collapse. It is clear that this structure eventually brings the condensation of domain sizes around $y = y_D(t)$. On the other hand, the potential $U_I(y; t)$ has a repulsive point at $y = y_D(t)$, where domain sizes for $y < y_D(t)$ diminish and collapse at $y = y_c$, and that for $y > y_D(t)$ grows, while $y > y_D(t)$ holds. In the analysis with the scaling hypothesis in Sec. V A, at Eq. (5.25), we have shown that the mean scaled domain size does not take any fixed value but diverges toward a negative infinity. This behavior is implied from the form of $U_B(y, Q; t)$ for $y \gg y_D(t)$, i.e., $U_B(y, Q; t) \sim 2e^{-y_D(t)}y$, by which domain sizes always flow out of the region $y \gg y_D(t)$, which was assumed to be scaling region in the analysis of Sec. V A. For the Néel wall situation, the DSDF obeys the scaling-type distribution. While the dynamical scaling structure is developed by the annihilation process, the stability of the scaling behavior is supported by the potential structure $U_I(y; t)$. This is intuitively explained by using Eq. (6.1): the equation of motion for the scaled domain size $Y = y/y_D(t)$, being written as

$$\dot{Y} = -\frac{\dot{y}_D(t)}{y_D(t)}Y + \frac{2}{y_D(t)}[e^{-y_D(t)} - e^{-y_D(t)Y}], \quad (6.4)$$

has a stable fixed point depending on the form of $\dot{y}_D(t)$ [it is reasonable to be $\dot{y}_D(t) \propto e^{-y_D(t)}$]; this retains the scaling property of the DSDF at the edge of the scaling region. This discussion is similar to the argument by Lifshitz, Slyozov, and Wagner [4,5] for the scaling solution for droplet size distribution in a binary mixture system, and also suggests that we can classify whether DSDFs obey scaling behavior

or solitonlike behavior by a mean field force (or potential) like used here in 1D domain coarsening systems.

Finally, let us discuss the self-consistency of the obtained DSDF for solitonlike behavior. The characteristic size $y_D(t)$ was defined by $\langle Qe^{-y} \rangle = -e^{-y_D(t)}$ and this relation should be held with the DSDF $f(y, Q; t)$. To know the average $\langle Qe^{-y} \rangle$ needs information for the entire DSDF or all the moments $\langle y^k \rangle_Q$ ($k=1, 2, \dots$) for $Q = \pm 1$. However, due to approximation procedures, our result $h(z)$ does not have enough accuracy to calculate such higher order moments; hence, the above-mentioned relation is not useful. Instead, let us consider the conditional second-order moment of domain size as defined by $\langle \delta y^2 \rangle_{-1, -1}$, which is also approximated as

$$\begin{aligned} & \int_{y_c}^{\infty} dy f(-1; t) f(y, -1; t) (y - \langle y \rangle)^2 \\ & \simeq \int_{y_c}^{\infty} dy h^{\infty}(y - y_D(t)) (y - \langle y \rangle)^2. \end{aligned} \quad (6.5)$$

Here, we use the saddle point approximation for $h^{\infty}(z)$, i.e., the saddle point for Eq. (5.48) is given as $z^* = -\ln a^{\infty}$, and around $z = z^*$

$$h^{\infty}(z) \propto h^{\infty}(z^*) \exp\left(-\frac{a^{\infty}}{2b^{\infty}} \delta z^2\right), \quad (6.6)$$

with $\delta z = z - z^*$. This leads to $\langle y \rangle_{-1, -1} \simeq y_D(t) + z^*$ and $\langle \delta y^2 \rangle_{-1, -1} \simeq \langle \delta z^2 \rangle_{-1, -1} \simeq a^{\infty}/b^{\infty}$. From the relations (5.35), (5.36), (5.41), and (5.42), we have $a^{\infty} \simeq 1 + e^{y_D(t)} \dot{y}_D(t)/2$ and $b^{\infty}/\langle \delta y^2 \rangle_{-1, -1} \simeq R_{-1, -1} \langle e^{-z} \rangle_{-1}/2$ for sufficiently large t [$a(s) \simeq a^{\infty}$, $b(s) \simeq b^{\infty}$]. In terms of $y_D(t)$ and $R_{-1, -1}$, the relation $\langle y \rangle_{-1, -1} \simeq a^{\infty}/b^{\infty}$ reads

$$\dot{y}_D(t) \simeq (R_{-1, -1} \langle e^{-z} \rangle_{-1} - 2) e^{-y_D(t)}. \quad (6.7)$$

This proposes a qualitative self-consistent condition for the solitonlike behavior, namely, the growth of $y_D(t)$ requires the condition $R_{-1, -1} \langle e^{-z} \rangle_{-1} > 2$. Hence, it turns out that the correlation coefficient $R_{-1, -1}$ must be positive, and the DSDF for $Q = -1$ has to be sufficiently asymmetric for the inversion $z \rightarrow -z$. The former signifies that the solitonlike behavior is inevitably connected to the nonvanishing correlation coefficient, and that the latter can be read as the asymmetry coming from the unidirectional motion of the solitonlike behavior.

VII. SUMMARY

We discussed the dynamics of the domain size distribution in the 1D anisotropic XY -spin model, and provided another scenario of an ordering process. First, we showed the role of the repulsive interaction in the domain wall dynamics. It turned out that the repulsive interaction between neighboring walls brings about the formation of clusters and the condensation of domain sizes around one characteristic size. While the role of the attractive one is to drive the coarsening process accompanied by the annihilation of domains.

Next, we discussed the dynamics of DSDF based on the

numerical results obtained from Eq. (2.5). Although the growth law for the mean domain size possesses the same logarithmic growth law as obtained for the Néel wall situation, the DSDF exhibits a quite different behavior from the Néel wall case. The DSDF can be characterized by solitonlike translational motion, in which the peak position of the DSDF grows logarithmically but its shape does not so change.

With the help of numerical results, we theoretically analyzed the DSDF in the Bloch case based on a kinetic equation for domain sizes. The probability function for the realization of a specified twistness arrangement for n -consecutive domains was obtained, and it agreed well with the numerically obtained result. The DSDF for a single domain was studied in two steps. First, assuming a scaling form for the DSDF, we proved that it is not described as the scaling-type distribution function. Next, incorporating the correlation effect between neighboring domain sizes, we obtained a qualitative Fokker-Planck equation and its solution describing the solitonlike behavior.

Finally, we discussed the difference between the Néel and Bloch walls systems. This argument suggests that the structure of a mean field potential classifies the long term behavior of the DSDF into two types. We also discussed the self-consistent condition for the solitonlike behavior.

In the present study, we have not deal with the thermal noise effect, which may be important for more practical application. This remains for future study.

ACKNOWLEDGMENTS

I would like to thank Professor H. Fujisaka and Dr. S. Miyazaki for their help and advice.

APPENDIX A

For the case $n \geq 2$, the right hand side of Eq. (4.16) can be divided into one linear term proportional to $f_n(\{Q\}_1^n; t)$ and the other terms, denoted by $\zeta_{n-1}(\tau)$, comprising of the lower hierarchical probability functions, $f_k(\{Q\}_1^k; t)$ ($k = n-1, \dots, 1$), as

$$\partial_{\tau} f_n(\{Q\}_1^n; \tau) = -D(\tau) f_n(\{Q\}_1^n; \tau) + \zeta_{n-1}(\tau), \quad (A1)$$

where $D(\tau) = 2[f_1(-1; \tau) - f_1(1; \tau)] = 2 \tanh(\tau)$, and

$$\begin{aligned} \zeta_{n-1}(\tau) = & - \sum_{k=1}^n f_{k-1}(\{Q\}_1^{k-1}; \tau) f_{n-k}(\{Q\}_{k+1}^n; \tau) \delta_{Q_k, 1} \\ & + \sum_{k=2}^{n-1} \sum_{Q', Q''} \delta_{Q_k, Q'} f_k(\{Q\}_1^{k-1}, Q'; \tau) \\ & \times f_{n-k+1}(Q'', \{Q\}_{k+1}^n; \tau) \\ & + f_1(-1; \tau) [f_{n-1}(\{Q\}_2^n; \tau) + f_{n-1}(\{Q\}_1^{n-1}; \tau)]. \end{aligned} \quad (A2)$$

The detail of the calculation of Eq. (A2) is shown in the last paragraph of this appendix. Furthermore, Eq. (A1) can be written in the integral form

$$f_n(\{Q\}_1^n; \tau) = W(\tau) f_n(\{Q\}_1^n; 0) + W(\tau) \int_0^\tau W(\tau')^{-1} \zeta_{n-1}(\tau') d\tau', \quad (\text{A3})$$

where $W(\tau) = \exp[-\int_0^\tau D(\tau') d\tau'] = 1/\cosh(\tau)^2$. This is the recursion relation connecting n th and $(n-1)$ th functions. Hence, the n -body probability function can be inductively obtained with the relation Eq. (A3) in order from the probability function for $n=1$, which is given by Eq. (4.19). The result after carrying out this procedure becomes Eq. (4.20) for the symmetric initial condition $f_n(\{Q\}_1^n; 0) = 1/2^n$.

The proof is based on the mathematical induction method. The case $n=1$ [Eq. (4.19)] accords with Eq. (4.20). Supposing Eq. (4.20) is the form of the lower hierarchical probability functions up to $(n-1)$ th order, and substituting them into Eq. (A2), we obtain

$$\zeta_{n-1}(\tau) = \frac{2}{(e^\tau + e^{-\tau})^{n+1}} \left[-(n-2) \sinh(\tau) - \cosh(\tau) \sum_{k=1}^n Q_k \right] \exp\left(-\tau \sum_{i=1}^n Q_i\right). \quad (\text{A4})$$

Substituting this and $f_n(\{Q\}_1^n; 0) = 1/2^n$ into Eq. (A3), then we find $f_n(\{Q\}_1^n; \tau)$ to be of the same form as Eq. (4.20). Therefore, it is proved that the form (4.20), which is obtained for the symmetric initial configuration, holds for a general number n .

The detail of the calculation of Eq. (A2): the first summation in the right hand side of Eq. (4.16) does not include the n -body functions but consists of the lower hierarchical functions, thus they are included in $\zeta_{n-1}(\tau)$ as the first summation in Eq. (A2). The last summation in Eq. (4.16) can be divided into the n -body function and the others as

$$\begin{aligned} & \sum_{k=1}^n \sum_{Q', Q''} \delta_{Q_k, Q' Q''} f_k(\{Q\}_1^{k-1}, Q'; \tau) f_{n-k+1}(Q'', \{Q\}_{k+1}^n; \tau) \\ &= \sum_{k=2}^{n-1} \sum_{Q', Q''} \delta_{Q_k, Q' Q''} f_k(\{Q\}_1^{k-1}, Q'; \tau) \\ & \quad \times f_{n-k+1}(Q'', \{Q\}_{k+1}^n; \tau) \\ & + \sum_{Q', Q''} \delta_{Q_1, Q' Q''} f_1(Q'; \tau) f_n(Q'', \{Q\}_2^n; \tau) \\ & + \sum_{Q', Q''} \delta_{Q_n, Q' Q''} f_n(\{Q\}_1^{n-1}, Q'; \tau) f_1(Q''; \tau). \end{aligned}$$

The first summation is included in $\zeta_{n-1}(\tau)$ as the second summation in Eq. (A2), and the last two summations are furthermore expanded as

$$\begin{aligned} & \sum_{Q'} f_1(Q'; \tau) f_n(Q_1 Q', \{Q\}_2^n; \tau) \\ & + \sum_{Q'} f_n(\{Q\}_1^{n-1}, Q' Q_n; \tau) f_1(Q'; \tau) \\ &= 2f_1(1; \tau) f_n(\{Q\}_1^n; \tau) + f_1(-1; \tau) [f_n(-Q_1, \{Q\}_2^n; \tau) \\ & \quad + f_n(\{Q\}_1^{n-1}, -Q_n; \tau)] \\ &= 2[f_1(1; \tau) - f_1(-1; \tau)] f_n(\{Q\}_1^n; \tau) + f_1(-1; \tau) \\ & \quad \times [f_{n-1}(\{Q\}_2^n; \tau) + f_{n-1}(\{Q\}_1^{n-1}; \tau)], \end{aligned}$$

where we have used $\sum_{Q'} f_n(Q_1, \{Q\}_2^n; \tau) = f_{n-1}(\{Q\}_2^n; \tau)$ in the last step. The first term is the first in the right hand side of Eq. (A1), and the second is the last in Eq. (A2). Hence, all terms in Eq. (A1) are confirmed.

APPENDIX B

The equations for the first moment M_1^Q is

$$\frac{\partial}{\partial \tau} M_1^1 = 1 - 2M_0^{-1}(M_1^1 - M_1^{-1}) + \beta[1 - 2M_0^1 M_0^{-1}], \quad (\text{B1})$$

$$\frac{\partial}{\partial \tau} M_1^{-1} = 2M_0^{-1}(M_1^1 - M_1^{-1}) + 2\beta M_0^{-1} M_0^1. \quad (\text{B2})$$

Taking the sum and difference from Eqs. (B1) and (B2), we get

$$\frac{\partial}{\partial \tau} [M_1^1 + M_1^{-1}] = 1 + \beta, \quad (\text{B3})$$

$$\frac{\partial}{\partial \tau} [M_1^1 - M_1^{-1}] = 1 + \beta - 4M_0^{-1}(M_1^1 - M_1^{-1}) - 4\beta M_0^{-1} M_0^1. \quad (\text{B4})$$

These yield

$$M_1^1 + M_1^{-1} = M_1^1(0) + M_1^{-1}(0) + (1 + \beta)\tau, \quad (\text{B5})$$

$$\begin{aligned} M_1^1 - M_1^{-1} &= \frac{4[M_1^1(0) - M_1^{-1}(0)]}{(1 + e^{2\tau})^2} + \frac{1}{(1 + e^{2\tau})^2} \\ & \quad \times \left[(1 + \beta) \left(\tau + \frac{1}{4} e^{4\tau} \right) - \frac{5}{4} + \frac{3}{4} \beta + (1 - \beta) e^{2\tau} \right], \end{aligned} \quad (\text{B6})$$

where we have used

$$\int_{\tau'}^\tau d\tau'' M_0^{-1} = \frac{1}{2} \ln \left[\frac{1 + e^{2\tau}}{1 + e^{2\tau'}} \right] \quad (\text{B7})$$

in the calculation of the second equation. For large τ , Eqs. (B5) and (B6) behave as $M_1^1 + M_1^{-1} \rightarrow (1 + \beta)\tau$ and $M_1^1 - M_1^{-1} \rightarrow (1 + \beta)/4$, respectively.

APPENDIX C

The formula (5.26) and the related equations in Sec. V B are constructed from the characteristic function for two variables y_1 and y_2 ,

$$\begin{aligned} \tilde{f}_2(q_1, q_2) &\equiv \langle e^{-q_1 y_1 - q_2 y_2} \rangle \\ &\equiv \int_{y_c}^{\infty} d\{y_1, y_2\} e^{-q_1 y_1 - q_2 y_2} f_2(y_1, y_2), \end{aligned} \quad (C1)$$

where indexes for Q variables are omitted for simplicity, and the joint PDF $f_2(y_1, y_2)$ is normalized so that its integral is unity. Let us expand the characteristic function $\tilde{f}_2(q_1, q_2)$ as

$$\begin{aligned} \langle e^{-q_1 y_1 - q_2 y_2} \rangle &= \langle e^{-q_1 y_1} \rangle \langle e^{-q_2 y_2} \rangle \\ &+ \tilde{H}_2(q_1, q_2) \langle e^{-q_1 y_1} \rangle \langle e^{-q_2 y_2} \rangle. \end{aligned} \quad (C2)$$

The function $\tilde{H}_2(q_1, q_2)$ involves the correlation effect. With the cumulant generating functions, which is defined by $\langle e^{-q_i y_i} \rangle \equiv e^{\Psi_1(q_i)}$ ($i=1,2$) and $\langle e^{-q_1 y_1 - q_2 y_2} \rangle \equiv e^{\Psi_2(q_1, q_2)}$ for one and two variables, the function $\tilde{H}_2(q_1, q_2)$ is rewritten as

$$\tilde{H}_2(q_1, q_2) = e^{\Psi_2(q_1, q_2) - \Psi_1(q_1) - \Psi_1(q_2)} - 1. \quad (C3)$$

Assuming the functions Ψ_1 and Ψ_2 are analytic around $q_1 = q_2 = 0$, together with the relations

$$\Psi_2(q_1, q_2) = \ln \left[1 + \sum_{n=1}^{\infty} \sum_{m=0}^n \frac{(-1)^n q_1^m q_2^{n-m}}{m!(n-m)!} \langle y_1^m y_2^{n-m} \rangle \right], \quad (C4)$$

$\Psi_1(q_1) = \Psi_2(q_1, 0)$ and $\psi_1(q_2) = \Psi_2(0, q_2)$, the function $\tilde{H}_2(q_1, q_2)$ is expanded as

$$\begin{aligned} \tilde{H}_2(q_1, q_2) &= \exp \left(\sum_{n,m=1}^{\infty} \frac{q_1^n q_2^m}{n!m!} A_{n,m} \right) - 1 \equiv \sum_{n,m=1}^{\infty} \frac{q_1^n q_2^m}{n!m!} B_{n,m} \\ &\equiv q_1 q_2 \tilde{C}_2(q_1, q_2), \end{aligned} \quad (C5)$$

where

$$A_{n,m} = \frac{\partial^{n+m}}{\partial q_1^n \partial q_2^m} \Psi_2(q_1, q_2) \Big|_{q_1=0, q_2=0}, \quad (C6)$$

and the coefficient $B_{n,m}$ is determined from the combination of $\{A_{n,m}\}$. A few particular cases of $B_{n,m}$ are as follows:

$$B_{1,1} = A_{1,1} = \tilde{C}_2(0,0) = \langle y_1 y_2 \rangle - \langle y_1 \rangle \langle y_2 \rangle, \quad (C7)$$

$$\begin{aligned} B_{1,2} = A_{1,2} &= -\langle y_1^2 y_2 \rangle + \langle y_1^2 \rangle \langle y_2 \rangle + 2\langle y_1 y_2 \rangle \langle y_2 \rangle \\ &- 2\langle y_1 \rangle^2 \langle y_2 \rangle. \end{aligned} \quad (C8)$$

The function $\tilde{C}_2(q_1, q_2)$ extracts the correlation effect between two variables. Applying the inverse Laplace transformation, which is defined as

$$f_2(y_1, y_2) = \frac{1}{(2\pi i)^2} \int_{-i\infty}^{i\infty} d\{q_1, q_2\} e^{q_1 y_1 + q_2 y_2} \tilde{f}_2(q_1, q_2), \quad (C9)$$

for Eq. (C1), to both sides of Eq. (C2), we obtain the joint PDF for y_1 and y_2 as

$$f_2(y_1, y_2) = f_1(y_1) f_1(y_2) + G_2(y_1, y_2), \quad (C10)$$

where $f_1(y_i)$ ($i=1,2$) is the single-variable PDF and $G_2(y_1, y_2)$ is defined by

$$\begin{aligned} G_2(y_1, y_2) &= \frac{\partial^2}{\partial y_1 \partial y_2} \int_{y_c}^{\infty} d\{y'_1, y'_2\} C(y_1 - y'_1, y_2 - y'_2) \\ &\times f_1(y'_1) f_1(y'_2), \end{aligned} \quad (C11)$$

with

$$C(Y_1, Y_2) = \frac{1}{(2\pi i)^2} \int_{-i\infty}^{i\infty} d\{q_1, q_2\} e^{q_1 Y_1 + q_2 Y_2} \tilde{C}(q_1, q_2). \quad (C12)$$

Here, $f_2(y_1, y_2)$ must satisfy the condition $\int_{y_c}^{\infty} dy_2 f_2(y_1, y_2) = f_1(y_1)$, and from Eq. (C10) this leads to $\int_{y_c}^{\infty} dy_2 G_2(y_1, y_2) = 0$. From the integration of Eq. (C11) on one of the two variables, we can find that such a relation is held by the function form

$$C(Y_1, Y_2) = C'(Y_1, Y_2) \theta(Y_1) \theta(Y_2), \quad (C13)$$

by introducing a function $C'(Y_1, Y_2)$. Supposing this form for $C(Y_1, Y_2)$, via the Laplace transformation of Eq. (C12), we have

$$\tilde{C}(q_1, q_2) = \int_0^{\infty} d\{Y_1, Y_2\} e^{-q_1 Y_1 - q_2 Y_2} C(Y_1, Y_2). \quad (C14)$$

Putting $q_1 = q_2 = 0$, this provides the useful sum rule

$$\tilde{C}(0,0) = \langle y_1 y_2 \rangle - \langle y_1 \rangle \langle y_2 \rangle = \int_0^{\infty} d\{Y_1, Y_2\} C(Y_1, Y_2). \quad (C15)$$

- [1] J.D. Gunton, M.S. Miguel, and P.S. Sahni, *Phase Transition and Critical Phenomena* (Academic Press, New York, 1983), Vol. 8, p. 267.
[2] H. Furukawa, *Adv. Phys.* **34**, 703 (1985).

- [3] A.J. Bray, *Adv. Phys.* **43**, 357 (1994).
[4] I.M. Lifshitz and V.V. Slyozov, *J. Phys. Chem. Solids* **19**, 35 (1961).
[5] C. Wagner, *Z. Elektrochem.* **65**, 581 (1961).

- [6] B. Derrida, C. Godr che, and I. Yekutieli, *Phys. Rev. A* **44**, 6241 (1991).
- [7] L.N. Bulaevskii and V.L. Ginzburg, *Zh. Eksp. Teor. Fiz.* **45**, 772 (1963) [*Sov. Phys. JETP* **18**, 530 (1964)].
- [8] H. Tutu and H. Fujisaka, *Phys. Rev. B* **50**, 9274 (1994).
- [9] T. Nagai and K. Kawasaki, *Physica A* **120**, 587 (1983).
- [10] K. Kawasaki and T. Nagai, *Physica A* **121**, 175 (1983).
- [11] T. Nagai and K. Kawasaki, *Physica A* **134**, 483 (1986).
- [12] K. Kawasaki, A. Ogawa, and T. Nagai, *Physica B* **149**, 97 (1988).
- [13] A.D. Rutenberg and A.J. Bray, *Phys. Rev. E* **50**, 1900 (1994).
- [14] S.N. Majumdar and D.A. Huse, *Phys. Rev. E* **52**, 270 (1995).
- [15] H. Ikeda, *J. Phys. Soc. Jpn.* **52**, 33 (1983).
- [16] H. Ikeda, *J. Phys. C* **16**, 3563 (1983).
- [17] H. Ikeda, *J. Phys. C* **19**, L535 (1986).
- [18] N. Metoki, H. Suematsu, Y. Murakami, Y. Ohishi, and Y. Fujii, *Phys. Rev. Lett.* **64**, 657 (1990).
- [19] A.D. Rutenberg and A.J. Bray, *Phys. Rev. Lett.* **74**, 3836 (1995).
- [20] K. Kawasaki and T. Ohta, *Physica A* **118**, 175 (1983).
- [21] H. Risken, *The Fokker-Planck Equation* (Springer-Verlag, Berlin, 1984).